Studies on porphyrin-based nanorods for artificial light harvesting applications

Nametso P. Mongwaketsi

Dissertation presented for the degree of PhD in Polymer Science

University of Stellenbosch

Promoter:
Prof. Malik Maaza

Co-promoters:
Prof. Bert Klumperman
Dr. Raymond Sparrow

April 2014

Declaration

By submitting this dissertation, I declare that the entirety of the work contained therein is my own, original work, that I am the owner of the copyright thereof (unless to the extent explicitly otherwise stated) and that I have not previously in its entirety or in part submitted it for obtaining any qualification.

Signature ……

Date: ……...

Abstract

The work presented in this thesis throws light on the supramolecular approach in exploration of bi-porphyrin nanorods system wherein self-assembly plays an important role. Porphyrin based nanorods were synthesized via self-assembly of *meso-tetrakis* (4-phenylsulfonicacid) porphyrin dihydrochloride and Sn (IV) *tetrakis* (4-pyridyl) porphyrin. Understanding the sizes and growth mechanism of the porphyrin nanorods by self-assembly and molecular recognition is essential for their successful implementation in nanodevices. Spectroscopic and microscopic studies were carried out to investigate the effect that time, concentration and solvents have on the fabrication of the porphyrin nanorods by ionic self- assembly. This study demonstrated that aggregates of the di- acid form of *meso-tetrakis* (4-phenylsulfonic acid) porphyrin dihydrochloride and Sn (IV) *tetrakis* (4-pyridyl) porphyrin resulted in porphyrin nanorods with diameters between 20 nm and 60 nm, and μm in lengths. Enhanced optical properties illustrated the potential for slightly modifying the method of synthesis to influence the physical and optical properties of porphyrin nanorods. The porphyrin nanorods reflectance data demonstrated that these structures are good absorbers of light and therefore could potentially be used to harvest light. The nonlinear optical (NLO) properties of the porphyrin nanorods were investigated for the first time in this study by second and third harmonic generation techniques. Such study was influenced by the fact that porphyrins have great thermal stability and extended π-conjugated macro cyclic ring which give them large nonlinear optical effects. The NLO results showed that the porphyrin nanorods may have many potential uses in photonic applications due to larger third order nonlinear susceptibility. Single molecule spectroscopy was also used to investigate the dynamics of intermolecular and intramolecular processes. Porphyrin nanorods were incorporated into polymer matrices to achieve an arrangement where they can be directly used as a device. The assembly of porphyrin nanorods on track-etched membranes was achieved through altering the surface charge of the respective membranes. Porphyrin nanorods-polymer composites were produced using latex technology and electrospinning techniques. The fibres were characterized with respect to morphology and optical properties.

Opsomming

Die werk wat in hierdie tesis beskryf word werp lig op die supramolekulêre benadering in die ondersoek van bi-porfirien nano-silinders waarin self-versameling ‘n belangrike rol speel. Porifirien nano-silinders was voorberei via self-versameling van meso-tetrakis(4-feniel sulfoonsuur) porfirien dihidrochloried en Sn (IV) terakis (4-piridiel) porfirien. Dit is belangrik om die meganismes wat verband hou met die groei en grootte van die nano-silinder struktuur te ondersoek. Dit het ‘n invloed op die self-versameling asook die uiteindelike toepassing. Spectroskopiese en mikroskopiese studies was uitgevoer om die effek van tyd, konsentrasie en oplosmiddel op die selfversamelling te bestudeer. Die studie dui daarop dat bondels van die di-suur vorm van meso-tetrakis(4-feniel sulfoonsuur) porfirien dihidrochloried en Sn (IV) terakis (4-piridiel) porfirien het gelei tot porfirien nano-silinders met lengtes tussen 20 nm en 60 nm asook in die mikro meter skaal. Verhoogde optiese eienskappe het die potensiaal om effense veranderinge in die metode om die nano-silinders voor te berei om sodoende ‘n groter invloed op die fisiese en optiese einskappe te hê. Die reflektansie data wys dat hierdie strukture goeie absorbsies van lig toon en daarom geskik sal wees om lig te stoor. Die nie-liniêre optisie (NLO) eienskappe van die profirien nano-silinders was vir die eerste keer ondersoek deur middel van tweed en derde hormoniese generasie tegnieke. Hierdie studie was beïnvloed deur die feit dat porfiriene goeie stabiliteit by hoë temperatuur en ‘n verlengde π-gekonjugeerde makro-sikliese ring bevat wat dan groot nie-liniêre optiese effekte gee. Die NLO resultate wys dat die profirien nano-silinders groot potensiaal het in die gebruik van fotoniese toepassings as gevolg van derde orde nie-liniêre vatbaarheid. Enkel molekuul spektroskopie was ook gebruik om die dinamika van intermolekulêre en intramolekulêre prosesse te ondersoek. Porfirien nano-silinders was geïnkorporeer in polimeer matrikse om ‘n eweredige verspreiding te verkry en om direk as ‘n toestel te gebruik. Die versameling van porfirien nano-silinders op baan-ingeëtse membrane was bereik deur die verandering in oppervlak lading van die membrane. Porfirien nano-silinder / polimeer samestellings was verkry deur lateks tegnologie en elektrospin tegnieke. Die vesels was gekarakteriseer in terme van morfologie en optiese eienskappe.

This thesis is dedicated to the late Rre Tsebe Richard Mokalaka and Mmamatebele Anna Mokalaka who turned 83 this year

Acknowledgments

I would like to first and foremost give all the glory to GOD who, without Him and the tremendous grace and mercy He has shown me throughout my life and throughout this research, none of this would have been possible.

There are many people I could acknowledge, in accordance with the tradition of writing a thesis. My road until here has been long and never certain. Many people have played significant roles that resulted in my arrival, and sometimes my survival. My gratitude is greater than my memory so I leave them all in my heart. Many family members, friends and colleagues have played contributing roles. Here I will mention the ones closest to this work.

Prof. Maaza, I am deeply grateful for his detailed and constructive comments and for his important support throughout this work.

I owe my most sincere gratitude to Prof. Bert Klumperman, who gave me the opportunity to work with him and would also like him for his patience, encouragement and for always having time to give guidance when needed.

Dr. Sparrow for his understanding, encouraging and personal guidance that provided a good basis for this thesis. He has been actively interested in this work and has always been available to advise me.

During this work I have collaborated with many colleagues for whom I have great regard, and I wish to extend my warmest thanks to all those who have helped me with my work:

Prof. Garab of Biological Research Center, Hungarian Academy of Sciences, and his Group for the opportunity to work with them and gave me untiring help during my visit.

Tomas Fessl of Lab of Single Molecule Spectroscopy at the University of South Bohemia for his help with the single molecular spectroscopy experiments.

Dr Anechaev and Dr Ndungu, Department of Chemistry, University of the Western Cape for their contribution in this work which resulted in a publication.

I want to thank Prof. Sahraoui of the Physics Department at the University of Angers for his assistance with NLO measurements, a collaboration which also resulted in a publication.

I would like to thank MRD staff and my fellow postgraduate students at iThemba LABS for the effort they made in promoting a stimulating and friendly academic and social environment.

Thank you to Dr Nemutudi who has always been ready and willing to provide help and support when I requested it.

I would also like to thank my colleagues and friends at the CSIR Biosciences-Synthetic biology group.

I would also like to extend my sincere gratitude to the Advanced Macromolecular Architecture group at the Polymer Science, Stellenbosch University. Many thanks to Dr. Pfukwa and Dr. Hlalele for their assistance and support.

My deep love and appreciation goes to Mokalaka family in the North West Province (Mareetsane & Mahikeng) for all the support and love that help me go through all these years from such a great distance. Sennelo, Botsile, Obuseng, Khumoeng, Modiri, Gaobakwe and all my cousins kealeboga go tlala seatla.

Thanks to my special mother Mary Mokalaka, for all the unconditional help and support since the very beginning of my career. "*Ke leboga go tswa kwa botennyeng jwa pelo"*

I would also like to say thanks to my one and only sister Kgomotso and her husband Jeff Matshoba for all the advices and support.

The undertaking of this project is a milestone in my life and I absolutely could not have reached it without the support of my sweetheart Given Mokwena.

It would be a long list to mention all the friends I am indebted to. I gratefully thank all of them.

CONTENTS

LIST OF FIGURES

LIST OF TABLES

LIST OF EQUATIONS

LIST OF PUBLICATIONS ARISING FROM THIS WORK

1. Ionic self-assembly of porphyrin nanostructures on the surface of charge-altered track-etched membranes
   N. Mongwaketsi, P. G. Ndungu, A. Nechaev, M. Maaza, R. Sparrow
   Journal of Porphyrins Phthalocyanines (2010) 14: 446–451

2. Synthesis and Characterization of Porphyrin Nanotubes/Rods for Solar Radiation Harvesting and Solar Cells
   N. Mongwaketsi, S. Khamlich, B. Klumperman, R.Sparrow, M. Maaza
   Physica B Condensed Matter (2012) 407 1615–1619

3. Physical origin of third order non-linear optical response of porphyrin nanorods
   N. Mongwaketsi, S. Khamlich, M. Pranaitis, B. Sahraoui, F. Khammarc, G. Garab, R. Sparrow, M. Maaza
   Journal of Materials Chemistry and Physics (2012) 134 646-650

4. Nonlinear photonics properties of porphyrins nanocomposites and self-assembled porphyrins
   M. Maaza, N. Mongwaketsi, M. Genene, G. Hailua, G. Garab, B. Sahraoui, D. Hamidi
   Journal of Porphyrins Phthalocyanines (2012) 16 1–11

INTRODUCTION

1.1. Background information

The demand for renewable sources of energy is increasing daily whilst non-renewable fossil fuels are being depleted [1]. Alternative sources of renewable energies include solar energy [2], biomass energy [3], wind and hydrogen energy [4]. The prospect of realizing artificial photosynthesis for harvesting solar energy has motivated many researchers [5-8]. The design of artificial photosynthetic systems requires several key factors, including absorption in the UV-visible and near-infrared wavelengths, energy transfer ability and the selection of light absorbing pigments. Another key factor is the organizational structure through which the components will interact. Within various natural and synthetic light harvesting complexes, light is absorbed by chlorophyll molecules followed by energy transfer (ET) to neighbouring molecules. This ET is the primary process in utilizing energy in the 450 – 550 nm wavelength range, and it contributes significantly to the functioning of the system [9]. A high priority, therefore, is placed on understanding the optical and structural properties of the natural ET systems in order to aid the development of efficient artificial systems [10-14]. A major driving force in the research on artificial light harvesting systems is to realise the conversion of solar energy into renewable clean energy [15-17]. Significant effort needs to be invested in the development of inexpensive and efficient light-harvesting materials. Porphyrin molecules have been shown to be promising candidates for artificial antenna systems [18-21]. They meet the requirements for efficient photosynthetic systems (*vide supra*) and are anticipated to produce a significant technological impact on solar cell industries.

In nature, chromophores are employed for the transfer of energy and electrons, and they are organized in a manner that facilitates the transfer of excitation energy or electrons rapidly and with high efficiency. A particular example is the structure of the circular light-harvesting antenna complex of purple bacteria [22]. The development of functional units that are able to self-assemble by having appropriate recognition sites is important in producing a functional artificial photosynthetic system [12]. The self-assembly approach has been adopted in the design and preparation of functional supramolecular materials [23]. Connecting these components in a manner that will allow their cooperation to efficiently harvest light energy and convert it to

chemical energy is a challenge [24]. Scientists at the Sandia laboratories have already shown that self-assembly leads to well-defined porphyrin nanotubes [25-29]. From other similar studies it was found that the porphyrin nanotubes produced retain the desirable properties of porphyrin self-aggregates and they may be expected to mimic the light-harvesting and photosynthetic functions of the chlorosomal rods [15,30,31].

1.2. Aims and objectives

This research is based on exploring the self-assembly of porphyrin "monomers" into rod-like nanostructures. The interest in porphyrins stems from their structural similarity to chlorophylls.

In nature, the precise organization and orientation of the chlorophylls result in efficient absorption of light energy. Inspired by these naturally occurring architectures, another focus of this research was the use of suitable solid matrices to host the porphyrin nanorods. The embedding of porphyrin nanorods in a solid matrix will improve their processability since porphyrin nanorods are difficult to handle when prepared in solution and degrade with long exposures to light. In the current study we attempted to accomplish this by exploring three approaches;

- ✓ The porphyrin nanorods were embedded in a polymeric (polystyrene) matrix, using latex technology. Although latex technology has been utilised in incorporating carbon nanotubes into polymer matrices, [32-36] this idea has not been utilised for porphyrin-based nanostructures.
- ✓ Self-assembly of porphyrin-based nanostructures on the surface of polyethyleneimine (PEI) membranes. The results from this investigation demonstrated how ionic interactions can induce porphyrin self-aggregation on a solid surface. This will be of important value in regard to approaches to fabricating nanostructures on solid substrates.
- ✓ Production and characterization of porphyrin nanostructures embedded in electrospun polymer nanofibres. This also gave the possibility of investigating the orientation of nanorods in the polymer and the interaction between them and the polymer matrix.

This thesis is structured as follow:

Chapter 1 introduces and provides the aims and objectives of the research.

Chapter 2 is the literature review covering:

- ✓ A general background on the properties of porphyrins, their roles in artificial systems as well as general applications.
- ✓ Porphyrin aggregates, factors that have an influence on the self-assembly process as well as related artificial systems.
- ✓ An overview on methods of incorporating nanoparticles in polymer matrices by latex blending, electrospinning and embedding on the surface of a track-etched membrane.

Chapter 3 is the experimental work covering:

- ✓ Porphyrin nanorods synthesis by ionic self-assembly as well as the effect of time, concentration and solvent.
- ✓ Single molecular spectroscopic investigation on porphyrin nanorods.

Chapter 4 is the experimental work covering the embedding of porphyrin nanorods in polymer matrices to produce composites by:

- ✓ Self-assembly on the surface of a membrane
- ✓ Latex blending
- ✓ Electrospinning

Chapter 5 is based on the potential application of porphyrin aggregate by studying the non-linear optical (NLO) properties of porphyrin nanorods.

Chapter 6 gives the overall conclusion based on the results obtained as well as recommendations for future research work in the same field.

1.3. References

[1] S. Shafiee and E. Topal, *Energ. Policy,* **37**, 181-189 (2009).

[2] M. Asif and T. Muneer, *Renew. Sust. Energ. Rev,* **11**, 1388-1413 (2007).

[3] M. Wackernagel, N.B. Schulz, D. Deumling, A.C. Linares, M. Jenkins, V. Kapos, C. Monfreda, J. Loh, N. Myers, and R. Norgaard, *Proc. Nat. Acad. Sci.,* **99**, 9266-9271 (2002).

[4] M.S. Dresselhaus and I.L. Thomas, *Natural gas,* **21**, 19-29 (2001).

[5] W.M. Campbell, K.W. Jolley, P. Wagner, K. Wagner, P.J. Walsh, K.C. Gordon, L. Schmidt-Mende, M.K. Nazeeruddin, Q. Wang, and M. Grätzel, *J. Phys. Chem. C.,* **111**, 11760-11762 (2007).

[6] T. Bessho, S.M. Zakeeruddin, C.Y. Yeh, E.W.G. Diau, and M. Grätzel, *Angew. Chem. Int. Ed.,* **49**, 6646-6649 (2010).

[7] J. Deisenhofer and J.R. Norris, *Eds. Academic Press, San Diego,* **2**, 179-220 (1993)

[8] D.R. Ort, C.F. Yocum, and I.F. Heichel,*Kluwer Academic Publications: Dordrecht, The Nertherland* 213-247 (1996).

[9] T. Hori, Y. Nakamura, N. Aratani, and A. Osuka, *J. Organomet. Chem.,* **692**, 148-155 (2007).

[10] D. Gust, T.A. Moore, and A.L. Moore, *Acc. Chem. Res.,* **42**, 1890-1898 (2009).

[11] P.V. Kamat, *J. Phys. Chem. B,* **111**, 2834-2860 (2007).

[12] M.R. Wasielewski, *J. Org. Chem.,* **71**, 5051-5066 (2006).

[13] T.S. Balaban, *Acc. Chem. Res.,* **38**, 612-623 (2005).

[14] K. Kalyanasundaram and M. Graetzel, *Curr. Opin. Biotechnol.,* **21**, 298-310 (2010).

[15] D.A. LaVan and J.N. Cha, *Proc. Natl. Acad. Sci. U. S. A,* **103**, 5251-5255 (2006).

[16] I. McConnell, G. Li, and G.W. Brudvig, *Chem. Biol.,* **17**, 434-447 (2010).

[17] M. Freemantle, *Chem. Eng. News,* **76**, 37-46 (1998).

[18] M.R. Wasielewski, *Acc. Chem. Res.,* **42**, 1910-1921 (2009).

[19] R.W. Wagner, T.E. Johnson, and J.S. Lindsey, *J. Am. Chem. Soc.,* **118**, 11166-11180 (1996).

[20] J.S. Hsiao, B.P. Krueger, R.W. Wagner, T.E. Johnson, J.K. Delaney, D.C. Mauzerall, G.R. Fleming, J.S. Lindsey, D.F. Bocian, and R.J. Donohoe, *J. Am. Chem. Soc.,* **118**, 11181-11193 (1996).

[21] J.P. Strachan, S. Gentemann, J. Seth, W.A. Kalsbeck, J.S. Lindsey, D. Holten, and D.F. Bocian, *J. Am. Chem. Soc.,* **119**, 11191-11201 (1997).

[22] R.J. Cogdell, A. Gall, and J. Köhler, *Q. Rev. Biophys.,* **39**, 227-324 (2006).

[23] B. Rybtchinski, E. Louise, and M.R. Wasielewski, *J. Phys. Chem. A,* **108**, 7497-7505 (2004).

[24] M. Sykora, K.A. Maxwell, J.M. DeSimone, and T.J. Meyer, *Proc. Natl. Acad. Sci. U. S. A.,* **97**, 7687-7691 (2000).

[25] C. Huang, L. Wen, H. Liu, Y. Li, X. Liu, M. Yuan, J. Zhai, L. Jiang, and D. Zhu, *Adv Mater,* **21**, 1721-1725 (2009).

[26] C.J. Medforth, Z. Wang, K.E. Martin, Y. Song, J.L. Jacobsen, and J.A. Shelnutt, *Chem.Commun.,* , 7261-7277 (2009).

[27] Z. Wang, K.J. Ho, C.J. Medforth, and J.A. Shelnutt, *Adv Mater,* **18**, 2557-2560 (2006).

[28] Z. Wang, C.J. Medforth, and J.A. Shelnutt, *J. Am. Chem. Soc.,* **126**, 15954-15955 (2004).

[29] Z. Wang, C.J. Medforth, and J.A. Shelnutt, *J. Am. Chem. Soc.,* **126**, 16720-16721 (2004).

[30] J.A. Elemans, R. van Hameren, R.J. Nolte, and A.E. Rowan, *Adv Mater,* **18**, 1251-1266 (2006).

[31] T.S. Balaban, A.D. Bhise, G. Bringmann, J. Bürck, C. Chappaz-Gillot, A. Eichhöfer, D. Fenske, D.C.G. Götz, M. Knauer, and T. Mizoguchi, *J. Am. Chem. Soc.,* **131**, 14480-14492 (2009).

[32] M.C. Hermant, M. Verhulst, A.V. Kyrylyuk, B. Klumperman, and C.E. Koning, *Composites Sci. Technol.,* **69**, 656-662 (2009).

[33] J. Yu, K. Lu, E. Sourty, N. Grossiord, C.E. Koning, and J. Loos, *Carbon,* **45**, 2897-2903 (2007).

[34] N. Grossiord, J. Loos, O. Regev, and C.E. Koning, *Chem. Mater.,* **18**, 1089-1099 (2006).

[35] J. Loos, A. Alexeev, N. Grossiord, C.E. Koning, and O. Regev, *Ultramicroscopy,* **104**, 160-167 (2005).

[36] N. Grossiord, H.E. Miltner, J. Loos, J. Meuldijk, B. Van Mele, and C.E. Koning, *Chem. Mater.,* **19**, 3787-3792 (2007).

LITERATURE REVIEW

2.1. General overview

The process of photosynthesis has driven researchers to seek ways to mimic its fundamental features in artificial systems. The primary event in photosynthesis is the absorption of light by chlorophyll. Chlorophyll is composed of a porphyrin ring, coordinated to a central magnesium atom, denoted as "M" in Figure 1. A significant research focus is now placed on understanding the basic processes of natural photosynthesis and on the construction of artificial systems that are able to mimic these processes [1-3]. An artificial photosynthetic system capable of converting solar energy into fuels should comprise of:

- An antenna for light harvesting,
- A reaction centre for charge separation,
- A proton reduction catalyst,
- A membrane to separate the generated products.

Charge separation refers to the process of an electron in an atom being excited to a higher energy level by the absorption of a photon and then leaving the atom onto a nearby electron acceptor. An antenna for light harvesting is an organized multi-component system in which several chromophoric molecular species absorb the incident light and channel the excitation energy to a common acceptor component [4]. The light-harvesting complex (LHC) of plants is an array of protein and chlorophyll molecules embedded in the thylakoid membrane, which transfer light energy to the reaction centre. Many purple bacteria have two types of light harvesting complexes (LHCs), denoted as LHC I and LHC II, in their photosynthetic membrane [5], with LHC I tightly bound to the reaction centre. LHC II is not directly associated with the reaction centre but transfers the energy to the reaction centres via LHC I [6]. LHC I and II are based on the same molecular structure [7] but LHC I is larger than LHC II because in the middle it has a reaction centre and accessory bacteriochlorophylls [8].

Herein we explore the applicability of porphyrin-based nanostructures as potential antennae for artificial light harvesting systems. Porphyrins have the characteristics required for light

harvesting systems. These include an extensive π-conjugated system, which increases their electron donating ability, light absorption ability in the visible, near-IR and IR regions of the electromagnetic spectra and long-lived excited states. *Meso*-tetra (p-sulfonatophenyl) porphyrins, for example, have a triplet lifetime of 2 μs [9] and have been shown to be stable in the oxidized, reduced and excited states, and resist photochemical degradation [10-12].

2.2. Porphyrins structural and optical properties

All porphyrins are derivatives of the parent methylene bridged tetra-pyrrolic macrocycle, porphine (Figure 1). Tetrapyrrole macrocycles occur widely in nature with many important biological representatives including chlorophylls. This tetra-pyrrolic macro-cycle is a highly conjugated aromatic system with 22 π electrons. The macrocycle has a central cavity, "M", that can incorporate a metal ion.

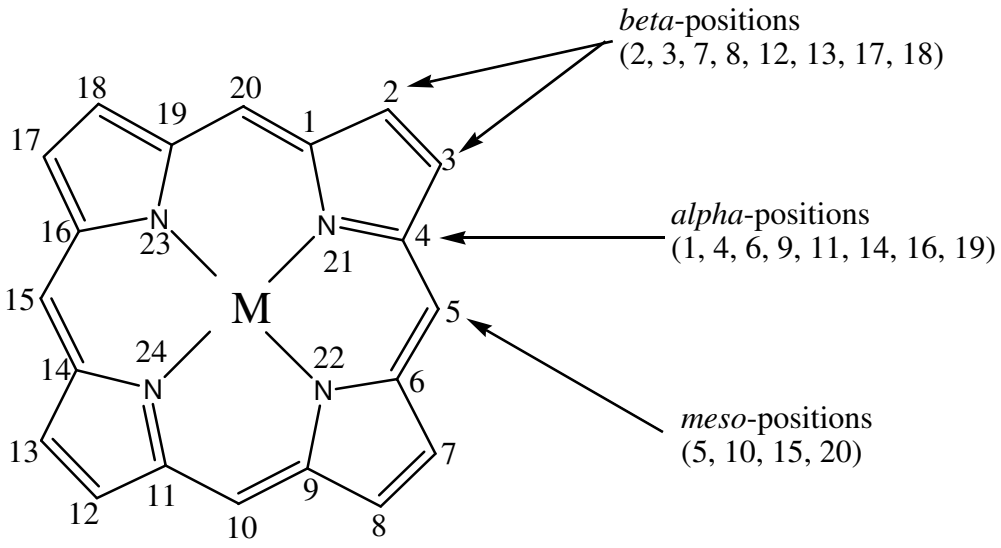

Figure 1. Structure of free-base porphyrin ring with its functionalization sites.

Porphyrins are generally soluble in water. However, the addition of suitable substituents can significantly change their solubility properties [13]. The substitutions can be made in the *beta* positions (at carbon atoms 2, 3, 7, 8, 12, 13, 17 and 18) or *meso*-positions (at carbon atoms 5, 10, 15 and 20).

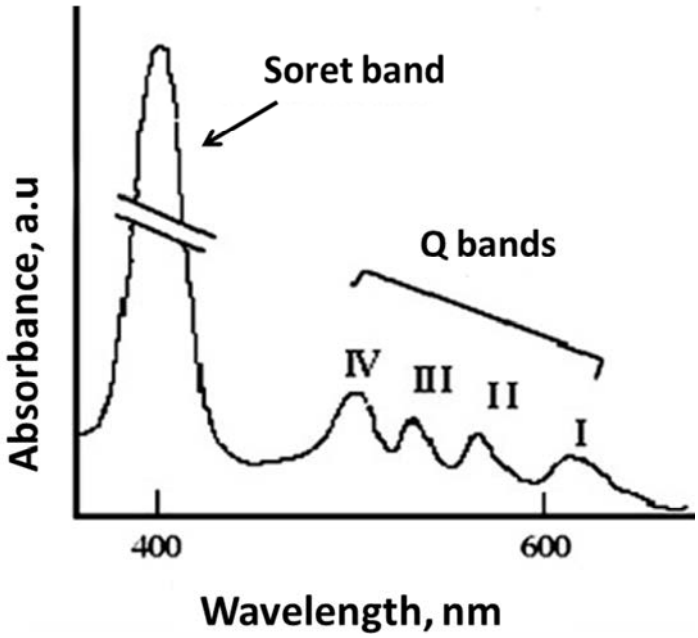

Figure 2. A typical UV-visible absorption spectrum of porphyrin [14]**.**

All visible absorption spectra of porphyrins display an exceedingly intense absorption band referred to as the "Soret" band between 380 and 420 nm. This is characteristic of the highly conjugated porphyrin macrocycle. The Soret band corresponds to the transition from the ground state (S_0) to the second excited singlet state (S_2) [15]. The visible absorption spectrum of the porphyrins also shows four weaker bands, the Q bands, at longer wavelengths from about 450-700 nm. These weaker absorption bands arise from the transition from the (S_0) state to the first singlet state (S_1). Porphyrins also possess strong fluorescence emission in the spectral region 600 – 750 nm which originates from the S_1 – S_0 transition. *Meso*-tetrakis (4-sulfonatophenyl) porphine ($TPPS_4$), which forms aggregates in acidic solution $H_2TPPS^{4-} + 2\ H^+ \leftrightarrow H_4TPPS^{2-}$), is one of the porphyrin monomers used in the present study, refer to Figure 3 for the structure. The

absorption spectrum of the tetraanion H_2TPPS^{4-} consists of an intense Soret peak at 412 nm and four Q-band peaks at 515, 552, 580 and 633 nm. The absorption spectrum of the dianion H_4TPPS^{2-} consists of a Soret band, which is intense and centred at 433 nm and two Q bands at 592 nm and 644 nm [16].

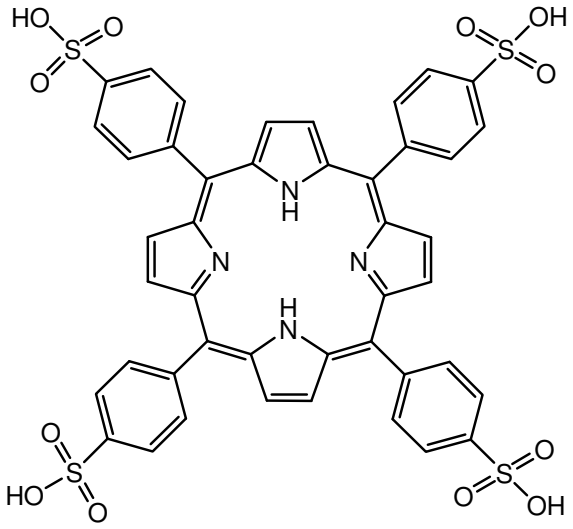

Figure 3. The structure of *meso*-tetrakis (4-sulfonatophenyl) porphyrin ($TPPS_4$).

2.3. Porphyrin aggregates by self-assembly

Non-covalent intermolecular forces can be used to engineer highly ordered three-dimensional macromolecular architectures in which the small molecule building blocks are held together by non–covalent interactions, such as metal-ligand binding, hydrogen bonding or π-π stacking [2,17-20]. Porphyrins have features that allow for molecular self-assembly as they have large, flat and π–conjugated surfaces, in the form of the tetrapyrrole macrocycles [18,21].

The self-assembly of porphyrins in solution into supramolecular structures, has been studied [22-33]. Porphyrins form two main types of aggregates in solution, the J-type and H-type, and they also form other non-specific aggregates, with features common to both J and H types [22]. The porphyrin molecules in J-aggregates are arranged side-by-side, whilst in H-aggregates the

arrangement is face-to-face [34,35]. In both J and H-aggregates, the monomers are arranged in a one–dimensional arrangement. In J-aggregates, the transition moments of monomers are parallel and the angle between the transition moments is zero. On the other hand, in H-aggregates the transition moments of the monomer are perpendicular to the line of centres. According to the excitonic splitting theory, H-aggregates exhibit a blue-shifted Soret absorption band, whereas J-aggregates are characterized by a red-shifted absorption band. For H_2TPPS_4, the interaction is via electrostatic attractions between the negatively charged sulfonate group and the central part of the positively charged porphyrin macrocycle.

2.4. Factors affecting porphyrin aggregation

Porphyrin aggregation in solution can be affected by the structure and substitution on the macrocycles. The pH and the ionic strength of the porphyrins also play a crucial role in aggregate formation. Kano *et al*. investigated $TPPS_4$ aggregation in water and found that aggregation is promoted when the porphyrin is in its di-acid monomeric form or when the ionic strength is increased [29]. Kubat and coworkers studied factors affecting the nature of *meso*-tetratolyl porphyrins aggregate, using UV-vis spectroscopy, and observed the temperature-induced J-aggregate-formation in which the porphyrin units were in a parallel arrangement, associated with the narrow, red-shifted Soret band [36]. Studies describing aggregation of tetraaryl-porphyrins have also been conducted, a typical example being 5,10,15,20-tetra sulfonatophenyl porphyrin, which forms J-aggregates in acidic solution [22,37]. The positively charged sites on this porphyrin macrocycle promote the electrostatic attraction to the negatively charged sulfonato groups, driving the aggregation process. The commercially available variants of this porphyrin derivative, 5,10,15,20-tetrakis (4-sulfonatophenyl) porphyrin, and 5,10,15,20-tetraphenylporphyrin Sn (IV) dichloride purchased from Frontier Scientific, were used in the present study.

2.5. Porphyrin aggregates in artificial systems

The self-assembly approach has been explored to construct systems that mimic photosynthetic processes. Endo *et al*. [38] self-assembled Zn porphyrin (ZnP) and free-base porphyrin (FbP) to construct an energy transfer system that was encapsulated inside Tobacco Mosaic Virus (TMV) structures. ZnP were used as donors and FbP as acceptors. The energy transfer from selectively excited zinc porphyrins took place through the Zn-porphyrin array to the free base porphyrin similar to natural light harvesting systems [39]. In another example, Hori *et al*. [40], utilised self-assembled porphyrin arrays as biomimetic models of light harvesting antenna in photosynthetic systems. These porphyrin ring molecules have been shown to serve as a platform to enable excitation energy transfer processes along the ring circuit with rates similar to those observed in natural cyclic photosynthetic antenna. Imahori *et al*. [41] also made an artificial photosynthetic system via self-assembly, and observed multiple electron transfer and photoinduced energy transfer events from the pyrene to the porphyrin with the conversion efficiency of 50 ± 8 %.Katterle *et al.*[42] reported on the functioning of their artificial photosynthetic unit in which self-assembled zinc chlorins (ZnChl) were used as light harvesting complexes. The structure of ZnChl is a porphyrin macrocycle with a central metal ion Zn instead of Mg. This study further demonstrated that self-assembly could be used to form supramolecular biomimetic light conversion units with 90 % conversion efficiency [42]. Wasielewski [43] developed bio-inspired building blocks that can serve to capture light energy, separate charge and transport charge throughout the system and explored how to self-assemble these building blocks. A molecule having four phenylenediamine (PDI) electron-accepting chromophores attached to a central zinc 5,10,15,20-tetraphenylporphyrin (ZnTPP) electron donor was self-assembled into ordered arrays. The process was driven by π-π interactions, which occurred both in solution and in the solid-state. Wasielewski [44] also designed and synthesized complex molecular systems, which comprised of electron donors and acceptors that mimic the charge separation function of the photosynthetic protein. They investigated photo-induced charge separation reactions as a means of capturing and storing solar energy. The results from Hung *et al*. [45]demonstrated that the yield of charge separation in multi-component molecular photovoltaics can be increased by a coordinated electron and proton transfer process.

Porphyrin aggregates have similar structures and properties as chlorophyll aggregates found in natural photosynthesis systems [44,46,47]. They are therefore seen as promising candidates for making artificial antenna systems and lend hope for use in solar cells [48]. In dye-sensitized solar cells (DSSCs), electron transfer from photo-excited dye molecules to substrates needs to be sufficiently fast, in order to compete effectively against loss processes, so as to achieve high solar energy conversion efficiencies. Molecular dyes, which are capable of photo-induced electron transfer, have been used to mimic the natural photosynthetic reaction centres in photochemical molecular devices. Porphyrins are among the most frequently used building blocks as electron donors and sensitizers in artificial photosynthetic models [49,50].

Porphyrin aggregates also have a significant thermal stability and an extended π-conjugated macro cyclic ring, which results in them having large nonlinear optical effects. Materials with such properties may be explored as field-responsive and as chemo-responsive materials [51]. In this study, the nonlinear optical response of porphyrin-based nanorods to second and third harmonic generation was explored.

Wang and co-workers produced porphyrin micro clovers by ionic self-assembly of $Zn^{II}T(N$-EtOH-4-Py)P^{4+} and photo-catalytic ($Sn^{IV}TPPS^{4-}$) complex of $TPPS_4$[28]. The porphyrin micro clovers produced, showed optical properties that make them suitable materials for sensing applications. They also produced porphyrin nanotubes that were shown to have good sensing properties for making gas sensors [52].

Porphyrin aggregates have also found use in photography for light harvesting. When these aggregates are adsorbed on silver halide grains they provide the photographic film with sensitivity to visible and infrared light [53].

2.6. Polymer matrix for nanoparticles incorporation

The use of nanoparticles as fillers in polymer matrices has been the area of research interest as they provide improved electrical, mechanical and thermal properties for the resulting composites

[54-59]. Various processing methods available for producing nanocomposites include melt mixing in which nanotubes are mixed with molten polymers using conventional processing techniques. A number of studies used melt mixing to investigate the dispersion state and the behaviour of nanoparticles in a polymer matrix [60-67].The other method is the solution mixing, whereby a solvent is used to dissolve the polymer and exfoliation of nanoparticles into uniform dispersion. This method has been used successfully to produce carbon nanotubes-polymer nanocomposites [68-72]. In-situ polymerization method, whereby nanoparticles are appropriately dispersed in the monomer solution followed by polymerization of the mixture [73,74], has also been used to generate nanocomposites [70].

In order to use porphyrin aggregates (in solution) for application as devices, their immobilization and incorporation into bulk materials such as polymers is essential [40]. For artificial light harvesting devices, lack of precise arrangement may have a negative impact on the efficiency of the system [75]. The orientation of these aggregates at a surface or in the bulk phase may have an influence on their performance in such applications. The difficulty of handling porphyrin aggregates in liquid solutions and their degradation with long exposure to light are also limiting factors for photonics applications. One of the approaches that have been used to improve porphyrin aggregates processability is to embed them onto a solid support [76-79]. In this research the porphyrin-based aggregates are embedded in a polymeric (polystyrene) matrix using latex technology. This technique provides an easier way to incorporate nanoparticles into a polymeric matrix due to the physical form of latexes, which is easy to handle and to be mixed with nanoparticles. Electrospinning is another technique explored with the aim of producing composites with improved properties. This technique also offers the possibility of orienting nanoparticles in polymer fibres. Self-assembly of nanoparticles on the surface of a modified track-etched membrane is another approach explored for the incorporation of nanoparticles onto a support. Ion-track etched membranes are usually synthesized by high energy ion irradiation of polycarbonate films coated on a conducting substrate [80].

In this work, polystyrene latex was used as the matrix surrounding and supporting the filler. Polystyrene is a widely used commercial polymer. Its use in filled polymer composites has been investigated extensively [56,63,81-91]. The common conductive fillers include ionic conductive polymers [92], conductive carbon black particles [93], and conductive nanotubes [71,85,94-97].

Carbon is the most commonly used filler for polymer matrix composites, resulting in composites with increased strength, thermal, and electronic properties [93,98]. Composites with homogenously dispersed carbon nanotubes produced by latex blending have attracted significant attention due to their outstanding mechanical properties [85,97,99,100]. Hermant *et al*. used this technique to study the incorporation of carbon nanotubes into polymeric matrices, to create conductive polymer-nanocomposites with low percolation threshold [101,102]. Various studies by Grossiord *et al.* [71,97,99] also employed this technique to incorporating single walled nanotubes (SWNTs) into a polymer matrix, using surfactants to disperse and exfoliate SWNTs in water by ultra-sonication. Regev *et al*. [72] used a similar approach to prepare conductive nanotube-polymer composites. Yu *et al*. [85] also produced conductive carbon nanotube/polystyrene composites using this technique. A percolation threshold of around 0.1 vol % was achieved for single-walled carbon nanotubes–polystyrene composites made by latex technology [103]. These studies demonstrate that the latex technology can be effectively applied to prepare polymer-carbon nanotube composites with good dispersion of carbon nanotubes [56,71,72,85].

2.6.1. Polymer-nanoparticles conductive composites

Many polymers (e.g. polystyrene) are non-conductive and can be used as insulating materials. Combinations of polymer materials and certain fillers result in the formation of composites, which, in some cases, have an improved conductivity [104]. The conductivity depends on the nature of the filler and its loading in the composite. When a critical filler concentration is reached, there is a sudden increase in the conductivity as a result of the formation of long-range connectivity in random systems. This phenomenon is referred to as the percolation threshold and it involves the transition from a non-connected to a connected state [105]. When the filler concentration is below the percolation threshold, the composite conductivity is almost the same as that of the polymer matrix, resulting in the composite remaining as an insulator. When the filler concentration reaches the percolation threshold concentration, the amount of filler becomes sufficient to form a continuous conductive network throughout the polymer matrix in which the

filler particles are in physical contact with each other [72,106-109]. The percolation theory was initially developed for spherical particles, however rod-shaped particles possess a higher aspect ratio and are therefore advantageous, as lower filler content is required to achieve percolation [110].

2.6.2. Electrospinning: polymer-nanoparticles fibres

Electrospinning is a technique that uses electrostatic forces to produce fibres from polymer solutions. The set-up of electrospinning experimental apparatus is shown in Figure 4. The diameters of fibres prepared by this method can range from tens of nanometers to several micrometers [111-115]. Electrospun polymer fibres with nanoparticles embedded on/in them are attractive composites due to improved mechanical, electrical and thermal properties [91,116-118].

2.6.2.1. Principles of electrospinning

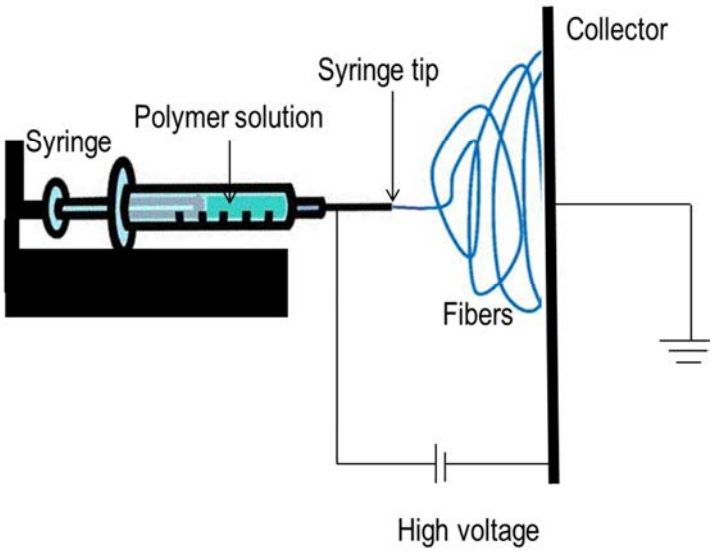

Figure 4. The horizontal set up of electrospinning experimental apparatus.

The main components of an electrospinning system are a syringe, with a needle that acts as one of the electrode to charge the polymer solution, the power supply to generate an electric field and a collector. An electrode is placed into the polymer solution and another onto the collector. Under the influence of the electric field, a charge is developed in the polymer solution. At low electric field strength, a hanging drop emerges out from the tip of the syringe containing the polymer solution, which is balanced by the surface tension of the solution. As the voltage increases, charges on the surface of the solution repel each other. This causes an elongation of the drop into a conical shape (Taylor cone) due to the electrostatic force, which is in the opposite direction to the surface tension. A jet of polymer solution is then ejected from the tip of the cone. The jet becomes thin as it travels to the counter electrode due to electrostatic repulsion between surface charge and due to solvent evaporation. Lastly, the solid fibres get deposited on the collector [115,119,120].

The fibres are usually deposited on the collector, as a non-woven mat, in a completely random orientation. This random orientation is a limiting factor in device fabrications for applications in photonic devices where well aligned and highly ordered architectures are required. A number of approaches for organizing the electrospun fibres into aligned arrays have been explored. These approaches include electrospinning using a rotating mandrel [120,121], a rotating disk [122], frame electrode [123], scanning tip [124] and wire drum [125] as well as the electric-magnetic field-induced technique [126]. For the current study the electric-magnetic field and rotating drum were used with an attempt to produce aligned electrospun fibres. When using a rotating drum as a collector, an aluminium foil attached to a drum, which is then rotated about its axis to generate a mat with preferential alignment of fibres along a specific direction. The rotating collector also produces dry fibres as it provides more time to the solvents to evaporate, enhancing fibre morphology [127].

2.6.2.2. Factors affecting the electrospinning process

Electrospinning parameters have a range in which they allow for stable electrospinning of polymeric solutions. However, due to the sensitivity of the fibre morphology to small changes in

these parameters, optimisation of these parameters is usually necessary for controlling the process in order to obtain the desired fibre morphologies and diameters.

In electrospinning, the molecular weight of the polymer is an important parameter, as it can be used to control the solution viscosity and the diameters of fibres produced [128,129]. Polymers with higher molecular weights have increased viscosity [130]. It is a challenge, however, to pump solutions with very high viscosity as they can dry at the needle tip. An advantage, however, of using higher molecular weight polymers is that the fibres produced have higher transition temperatures and better mechanical properties [131-133].

Another parameter is the distance between the Taylor cone and the collector, which can be varied, altering the flight distance as well as the electric field strength for a given voltage. When this distance is short, the flight path will be reduced and the field strength, which accelerates the jet downwards, will be increased. As a result there may not be sufficient time for the solvent to evaporate resulting in the formation of wet fibres, which can form either an interconnected fibre mesh or a polymer film. This is undesirable. Beaded fibres may also form due to the increased field strength, which, when it is too high, can cause instability in the jet and lead to the formation of beads. It is essential, therefore, to find the optimum Taylor cone tip to collector distance which is sufficient to enable evaporation of the solvent from the fibres whilst enabling formation of a stable jet that stretches out the fibres as much as possible [119].

Great progress has been made in producing electrospun nanoparticles-polymer fibres, and there are reports on the morphologies of pure electrospun nanofibres [112,134,135]. However, the morphologies of electrospun fibres embedded with carbon nanotubes and the interaction between carbon nanotubes and the polymer matrix have not been understood in depth.

Ko *et al.*[136] used the electrospinning process to prepare carbon nanotubes-filled nanofibres and reported thermal stability and reinforcement effect at less than 3 % volume single-walled carbon nanotubes. Another study was by Chang *et al.* [9], they prepared single-walled carbon nanotubes-polyvinylidene fluoride fibres and investigated their insulator-to-conductor transition properties. Using the same technique Dror and Salalha *et al.* [137,138] achieved well-dispersed single and multi-walled carbon nanotubes in electrospun PEO fibres.

Since the nanofibres are only several tens to hundreds of nanometers in diameter it is easy to observe them under an electron microscope [137]. We used the electrospinning method to

prepare porphyrin nanorods–PEO and porphyrin nanorods–polystyrene composite fibres. The voltage was varied in this study, and since it leads to the stretching of the fibres, anisotropy of the polymer matrix and probably also of the nanorods can be expected. Due to the size of the electrospun fibres, it is possible to study the orientation of nanorods in the polymer and the interaction between them and the polymer matrix.

2.7. References

[1] M.S. Choi, T. Yamazaki, I. Yamazaki, and T. Aida, *Angew. Chem. Int. Ed.,* **43**, 150-158 (2004).

[2] T.S. Balaban, A.D. Bhise, M. Fischer, M. Linke-Schaetzel, C. Roussel, and N. Vanthuyne, *Angew. Chem. Int. Ed.,* **42**, 2140-2144 (2003).

[3] D.A. LaVan and J.N. Cha,*Proc. Natl. Acad. Sci.,* **103**, 5251-5255 (2006).

[4] V. Balzani, A. Juris, H. Venturi, S. Campagna, S. Serroni, and G. Denti, *Sol. Energ. Mat. Sol.,* **38**, 159-173 (1995).

[5] C.J. Law, A.W. Roszak, J. Southall, A.T. Gardiner, N.W. Isaacs, and R.J. Cogdell, *Mol. Membr. Biol.,* **21**, 183-191 (2004).

[6] R.J. Cogdell, A. Gall, and J. Köhler, *Q. Rev. Biophys.,* **39**, 227-324 (2006).

[7] R.J. Cogdell, N.W. Isaacs, A.A. Freer, T.D. Howard, A.T. Gardiner, S.M. Prince, and M.Z. Papiz, *FEBS Lett.,* **555**, 35-39 (2003).

[8] X. Hu, A. Damjanović, T. Ritz, and K. Schulten, *Proc. Natl. Acad. Sci.,* **95**, 5935-5941 (1998).

[9] J.E. Roberts, S.J. Atherton, and J. Dillon, *Photochem. Photobiol.,* **54**, 855-857 (1991).

[10] S.M. Ribeiro, A.C. Serra, and A.M.A. Rocha Gonsalves, *Tetrahedron,* **63**, 7885-7891 (2007).

[11] G. Mele, R. del Sole, G. Vasapollo, E. García-López, L. Palmisano, L. Jun, R. Słota, and G. Dyrda, *Res. Chem. Intermediat.,* **33**, 433-448 (2007).

[12] D.B. Berezin, E.N. Mis' ko, E.V. Antina, and M.B. Berezin, *Russ. J. Gen. Chem.,* **76**, 482-487 (2006).

[13] X. Huang, K. Nakanishi, and N. Berova, *Chirality,* **12**, 237-255 (2000).

[14] L.B. Josefsen and R.W. Boyle, *Theranostics,* **2**, 916-966 (2012).

[15] V.N. Nemykin and R.G. Hadt, *J. Phys. Chem. A,* **114**, 12062-12066 (2010).

[16] N.C. Maiti, S. Mazumdar, and N. Periasamy, *J. Phys. Chem. B,* **102**, 1528-1538 (1998).

[17] C.M. Drain, F. Nifiatis, A. Vasenko, and J.D. Batteas, *Angew. Chem. Int. Ed.,* **37**, 2344-2347 (1998).

[18] C.M. Drain, I. Goldberg, I. Sylvain, and A. Falber, *Top Curr. Chem.* 55-88 (2005).

[19] C.M. Drain,*Proc. Natl. Acad. Sci.,* **99**, 5178-5182 (2002).

[20] X. Shi, K.M. Barkigia, J. Fajer, and C.M. Drain, *J. Org. Chem.,* **66**, 6513-6522 (2001).

[21] S.C. Doan, S. Shanmugham, D.E. Aston, and J.L. McHale, *J. Am. Chem. Soc.,* **127**, 5885-5892 (2005).

[22] N. Micali, F. Mallamace, A. Romeo, R. Purrello, and L. Monsù Scolaro, *J. Phys. Chem. B,* **104**, 5897-5904 (2000).

[23] R.F. Pasternack, K.F. Schaefer, and P. Hambright, *Inorg. Chem.,* **33**, 2062-2065 (1994).

[24] R. Rubires, J. Crusats, Z. El-Hachemi, T. Jaramillo, M. López, E. Valls, J.A. Farrera, and J.M. Ribó, *New J.Chem.,* **23**, 189-198 (1999).

[25] S.B. Brown, M. Shillcock, and P. Jones, *Biochem. J.,* **153**, 279-285 (1976).

[26] J.A.A.W. Elemans, R. van Hameren, R.J.M. Nolte, and A.E. Rowan, *Adv Mater,* **18**, 1251-1266 (2006).

[27] Z. Wang, K.J. Ho, C.J. Medforth, and J.A. Shelnutt, *Adv Mater,* **18**, 2557-2560 (2006).

[28] Z. Wang, C.J. Medforth, and J.A. Shelnutt, *J. Am. Chem. Soc.,* **126**, 15954-15955 (2004).

[29] K. Kano, K. Fukuda, H. Wakami, R. Nishiyabu, and R.F. Pasternack, *J. Am. Chem. Soc.,* **122**, 7494-7502 (2000).

[30] T.S. Balaban, *Acc. Chem. Res.,* **38**, 612-623 (2005).

[31] M. De Napoli, S. Nardis, R. Paolesse, M.G.H. Vicente, R. Lauceri, and R. Purrello, *J. Am. Chem. Soc.,* **126**, 5934-5935 (2004).

[32] J.M. Ribó, J. Crusats, J. Farrera, and M.L. Valero, *J. Chem. Soc., Chem. Commun.,* 681-682 (1994).

[33] J.M. Ribó, J. Farrera, M.L. Valero, and A. Virgili, *Tetrahedron,* **51**, 3705-3712 (1995).

[34] P.W. Bohn, *Annu. Rev. Phys. Chem.,* **44**, 37-60 (1993).

[35] A. Tonizzo, M. Cerminara, G. Macchi, F. Meinardi, N. Periasamy, P. Sozzani, and R. Tubino, *Synth. Met.,* **155**, 291-294 (2005).

[36] P. Kubát, K. Lang, K. Procházková, and P. Anzenbacher Jr, *Langmuir,* **19**, 422-428 (2003).

[37] S.C.M. Gandini, V.E. Yushmanov, I.E. Borissevitch, and M. Tabak, *Langmuir,* **15**, 6233-6243 (1999).

[38] M. Endo, M. Fujitsuka, and T. Majima, *Chem. Eur. J.,* **13**, 8660-8666 (2007).

[39] R.W. Wagner, T.E. Johnson, and J.S. Lindsey, *J. Am. Chem. Soc.,* **118**, 11166-11180 (1996).

[40] T. Hori, Y. Nakamura, N. Aratani, and A. Osuka, *J. Organomet. Chem.,* **692**, 148-155 (2007).

[41] H. Imahori, T. Umeyama, and S. Ito, *Acc. Chem. Res.,* **42**, 1809-1818 (2009).

[42] M. Katterle, V.I. Prokhorenko, A.R. Holzwarth, and A. Jesorka, *Chem. Phys. Lett.,* **447**, 284-288 (2007).

[43] M.R. Wasielewski, *J. Org. Chem.,* **71**, 5051-5066 (2006).

[44] M.R. Wasielewski, *Acc. Chem. Res.,* **42**, 1910-1921 (2009).

[45] S.C. Hung, A.N. Macpherson, S. Lin, P.A. Liddell, G.R. Seely, A.L. Moore, T.A. Moore, and D. Gust, *J. Am. Chem. Soc.,* **117**, 1657-1658 (1995).

[46] J.S. Hsiao, B.P. Krueger, R.W. Wagner, T.E. Johnson, J.K. Delaney, D.C. Mauzerall, G.R. Fleming, J.S. Lindsey, D.F. Bocian, and R.J. Donohoe, *J. Am. Chem. Soc.,* **118**, 11181-11193 (1996).

[47] J.P. Strachan, S. Gentemann, J. Seth, W.A. Kalsbeck, J.S. Lindsey, D. Holten, and D.F. Bocian, *J. Am. Chem. Soc.,* **119**, 11191-11201 (1997).

[48] M.S. Dresselhaus and I.L. Thomas, *Nat. Gas,* **21**, 19-29 (2001).

[49] W.M. Campbell, A.K. Burrell, D.L. Officer, and K.W. Jolley, *Coord. Chem. Rev.,* **248**, 1363-1379 (2004).

[50] M.K. Nazeeruddin, R. Humphry-Baker, L. David, W.M. Campbell, A.K. Burrell, and M. Grätzel, *Langmuir,* **20**, 6514-6517 (2004).

[51] K.S. Suslick, N.A. Rakow, M.E. Kosal, and J.H. Chou, *J. Porphyr. Phthalocya.,* **4**, 407-413 (2000).

[52] S. Valentinas, I. Bruzaite, and V. Lendraitis, *Microelectron. Eng.,* (2011).

[53] K. Kalyanasundaram and M. Grätzel, *Coord. Chem. Rev.,* **177**, 347-414 (1998).

[54] J. Hong, L. Schadler, R. Siegel, and E. Martensson, *Appl. Phys. Lett.,* **82**, 1956-1958 (2003).

[55] D. Kumlutas and I.H. Tavman, *J. Thermoplast. Compos. Mater.,* **19**, 441-455 (2006).

[56] M. Moniruzzaman and K.I. Winey, *Macromolecules,* **39**, 5194-5205 (2006).

[57] B. Zhu, S. Xie, Z. Xu, and Y. Xu, *Composites Sci. Technol.,* **66**, 548-554 (2006).

[58] M.A. Rafiee, J. Rafiee, Z. Wang, H. Song, Z. Yu, and N. Koratkar, *ACS nano,* **3**, 3884-3890 (2009).

[59] Tjong, *Mater. Sci. Eng. R-Rep.,* **53**, 73-197 (2006).

[60] P. Pötschke, A.R. Bhattacharyya, and A. Janke, *Polymer,* **44**, 8061-8069 (2003).

[61] Z. Zhang, J. Zhang, P. Chen, B. Zhang, J. He, and G.H. Hu, *Carbon,* **44**, 692-698 (2006).

[62] P. Pötschke, A.R. Bhattacharyya, and A. Janke, *Polymer,* **44**, 8061-8069 (2003).

[63] R. Haggenmueller, H. Gommans, A. Rinzler, J.E. Fischer, and K. Winey, *Chem. Phys. Lett.,* **330**, 219-225 (2000).

[64] M. Manchado, L. Valentini, J. Biagiotti, and J. Kenny, *Carbon,* **43**, 1499-1505 (2005).

[65] P. Pötschke, A.R. Bhattacharyya, and A. Janke, *Polymer,* **44**, 8061-8069 (2003).

[66] E.T. Thostenson and T. Chou, *J. Phys. D,* **35**, 77-80 (2002).

[67] T. Chang, A. Kisliuk, S. Rhodes, W. Brittain, and A. Sokolov, *Polymer,* **47**, 7740-7746 (2006).

[68] J.N. Coleman, U. Khan, W.J. Blau, and Y.K. Gun'ko, *Carbon,* **44**, 1624-1652 (2006).

[69] C.A. Mitchell, J.L. Bahr, S. Arepalli, J.M. Tour, and R. Krishnamoorti, *Macromolecules,* **35**, 8825-8830 (2002).

[70] B. Zhang, R.W. Fu, M.Q. Zhang, X.M. Dong, P.L. Lan, and J.S. Qiu, *Sensors Actuators B: Chem.,* **109**, 323-328 (2005).

[71] N. Grossiord, H.E. Miltner, J. Loos, J. Meuldijk, B. Van Mele, and C.E. Koning, *Chem. Mater.,* **19**, 3787-3792 (2007).

[72] O. Regev, P.N.B. ElKati, J. Loos, and C.E. Koning, *Adv Mater,* **16**, 248-251 (2004).

[73] X. Jiang, Y. Bin, and M. Matsuo, *Polymer,* **46**, 7418-7424 (2005).

[74] C. Park, Z. Ounaies, K.A. Watson, R.E. Crooks, J. Smith Jr, S.E. Lowther, J.W. Connell, E.J. Siochi, J.S. Harrison, and T.L.S. Clair, *Chem. Phys. Lett.,* **364**, 303-308 (2002).

[75] R.W. Wagner, T.E. Johnson, and J.S. Lindsey, *J. Am. Chem. Soc.,* **118**, 11166-11180 (1996).

[76] K. Peng, S. Chen, and W. Fann, *J. Am. Chem. Soc.,* **123**, 11388-11397 (2001).

[77] Q. Wang, W.M. Campbell, E.E. Bonfantani, K.W. Jolley, D.L. Officer, P.J. Walsh, K. Gordon, R. Humphry-Baker, M.K. Nazeeruddin, and M. Grätzel, *J. Phys. Chem. B,* **109**, 15397-15409 (2005).

[78] C. Xing, Q. Xu, H. Tang, L. Liu, and S. Wang, *J. Am. Chem. Soc.,* **131**, 13117-13124 (2009).

[79] R. Lauceri, A. Raudino, L.M. Scolaro, N. Micali, and R. Purrello, *J. Am. Chem. Soc.,* **124**, 894-895 (2002).

[80] L. Dauginet-De Pra, E. Ferain, R. Legras, and S. Demoustier-Champagne, *Nucl. Instr. Meth. Phys. Res. B,* **196**, 81-88 (2002).

[81] N.G. Sahoo, S. Rana, J.W. Cho, L. Li, and S.H. Chan, *Prog. Polym. Sci.,* **35**, 837-867 (2010).

[82] H. Miyagawa, M. Misra, and A.K. Mohanty, *J. Nanosci. Nanotechnol.,* **5**, 1593-1615 (2005).

[83] M. Paiva, B. Zhou, K. Fernando, Y. Lin, J. Kennedy, and Y.P. Sun, *Carbon,* **42**, 2849-2854 (2004).

[84] X. Gong, J. Liu, S. Baskaran, R.D. Voise, and J.S. Young, *Chem. Mat.,* **12**, 1049-1052 (2000).

[85] J. Yu, K. Lu, E. Sourty, N. Grossiord, C.E. Koning, and J. Loos, *Carbon,* **45**, 2897-2903 (2007).

[86] D.K. Woo, B.C. Kim, and S.J. Lee, *Korea-Aust Rheol. J.,* **21**, 185-191 (2009).

[87] T.M. Wu and E.C. Chen, *Composites Sci. Technol.,* **68**, 2254-2259 (2008).

[88] V. Antonucci, G. Faiella, M. Giordano, L. Nicolais, and G. Pepe, *Macromol. Symp.* **247**, 172-181 (2007).

[89] T.E. Chang, A. Kisliuk, S.M. Rhodes, W.J. Brittain, and A.P. Sokolov, *Polymer,* **47**, 7740-7746 (2006).

[90] H.J. Jin, H.J. Choi, S.H. Yoon, S.J. Myung, and S.E. Shim, *Chem. Mater.,* **17**, 4034-4037 (2005).

[91] L. Jin, C. Bower, and O. Zhou, *Appl. Phys. Lett.,* **73**, 1197 (1998).

[92] V. Dudler, M.C. Grob, and D. Mérian, *Polym. Degrad. Stab.,* **68**, 373-379 (2000).

[93] D.D.L. Chung, *Carbon fiber composites,* Butterworth-Heinemann, Newton, MA(1994).

[94] J. Loos, A. Alexeev, N. Grossiord, C.E. Koning, and O. Regev, *Ultramicroscopy,* **104**, 160-167 (2005).

[95] J.Z. Kovacs, K. Andresen, J.R. Pauls, C.P. Garcia, M. Schossig, K. Schulte, and W. Bauhofer, *Carbon,* **45**, 1279-1288 (2007).

[96] N. Grossiord, J. Loos, O. Regev, and C.E. Koning, *Chem. Mater.,* **18**, 1089-1099 (2006).

[97] N. Grossiord, J. Loos, and C.E. Koning, *J. Mater. Chem.,* **15**, 2349-2352 (2005).

[98] K. Miyasaka, K. Watanabe, E. Jojima, H. Aida, M. Sumita, and K. Ishikawa, *J. Mater. Sci.,* **17**, 1610-1616 (1982).

[99] N. Grossiord, J. Loos, O. Regev, and C.E. Koning, *Chem. Mater.,* **18**, 1089-1099 (2006).

[100] J. Yu, N. Grossiord, C.E. Koning, and J. Loos, *Carbon,* **45**, 618-623 (2007).

[101] M. Hermant, L. Klumperman, A. Kyrylyuk, P. Van Der Schoot, and C. Koning, *Soft Matter, 5, 878-885* (2009).

[102] M.C. Hermant, M. Verhulst, A.V. Kyrylyuk, B. Klumperman, and C.E. Koning, *Composites Sci. Technol.,* **69**, 656-662 (2009).

[103] D.S. McLachlan, C. Chiteme, C. Park, K.E. Wise, S.E. Lowther, P.T. Lillehei, E.J. Siochi, and J.S. Harrison,*J. Polym. Sci., Part B: Polym. Phys,* **43**, 3273-3287 (2005).

[104] G. Ruschau, S. Yoshikawa, and R. Newnham, *J. Appl. Phys.,* **72**, 953-959 (1992).

[105] V.K. Shante and S. Kirkpatrick, *Adv. Phys.,* **20**, 325-357 (1971).

[106] J. Sandler, M. Shaffer, T. Prasse, W. Bauhofer, K. Schulte, and A. Windle, *Polymer,* **40**, 5967-5971 (1999).

[107] F. Gubbels, R. Jérôme, P. Teyssie, E. Vanlathem, R. Deltour, A. Calderone, V. Parente, and J. Brédas, *Macromolecules,* **27**, 1972-1974 (1994).

[108] F. Du, R.C. Scogna, W. Zhou, S. Brand, J.E. Fischer, and K.I. Winey, *Macromolecules,* **37**, 9048-9055 (2004).

[109] H.G. Yoon, K.W. Kwon, K. Nagata, and K. Takahashi, *Carbon,* **42**, 1877-1879 (2004).

[110] F.H. Gojny, M.H.G. Wichmann, B. Fiedler, I.A. Kinloch, W. Bauhofer, A.H. Windle, and K. Schulte, *Polymer,* **47**, 2036-2045 (2006).

[111] N. Bhardwaj and S.C. Kundu, *Biotechnol. Adv.,* **28**, 325-347 (2010).

[112] H. Fong, I. Chun, and D. Reneker, *Polymer,* **40**, 4585-4592 (1999).

[113] P. Gupta, C. Elkins, T.E. Long, and G.L. Wilkes, *Polymer,* **46**, 4799-4810 (2005).

[114] D.H. Reneker and I. Chun, *Nanotechnology,* **7**, 216-223 (1996).

[115] J. Doshi and D.H. Reneker, *J. Electrostatics,* **35**, 151-160 (1995).

[116] Z. Zhou, C. Lai, L. Zhang, Y. Qian, H. Hou, D.H. Reneker, and H. Fong, *Polymer,* **50**, 2999-3006 (2009).

[117] J.N. Coleman, U. Khan, W.J. Blau, and Y.K. Gun'ko, *Carbon,* **44**, 1624-1652 (2006).

[118] J. Hwang, J. Muth, and T. Ghosh, *J Appl Polym Sci,* **104**, 2410-2417 (2007).

[119] T. Subbiah, G. Bhat, R. Tock, S. Parameswaran, and S. Ramkumar, *J Appl Polym Sci,* **96**, 557-569 (2005).

[120] B. Sundaray, V. Subramanian, T. Natarajan, R.Z. Xiang, C.C. Chang, and W.S. Fann, *Appl. Phys. Lett.,* **84**, 1222-1224 (2004).

[121] S.C. Moon, J.K. Choi, and R.J. Farris, *Fibre Polym.,* **9**, 276-280 (2008).

[122] A. Theron, E. Zussman, and A. Yarin, *Nanotechnology,* **12**, 384-390 (2001).

[123] R. Dersch, T. Liu, A. Schaper, A. Greiner, and J. Wendorff, *J. Polym. Sci., Part A: Polym. Chem.,* **41**, 545-553 (2003).

[124] J. Kameoka, R. Orth, Y. Yang, D. Czaplewski, R. Mathers, G.W. Coates, and H. Craighead, *Nanotechnology,* **14**, 1124-1129 (2003).

[125] P. Katta, M. Alessandro, R. Ramsier, and G. Chase, *Nano Lett.,* **4**, 2215-2218 (2004).

[126] J.A. Ajao, A.A. Abiona, S. Chigome, A. Fasasi, G. Osinkolu, and M. Maaza, *J. Mater. Sci.,* **45**, 2324-2329 (2010).

[127] P. Katta, M. Alessandro, R. Ramsier, and G. Chase, *Nano Lett.,* **4**, 2215-2218 (2004).

[128] C.L. Casper, J.S. Stephens, N.G. Tassi, D.B. Chase, and J.F. Rabolt, *Macromolecules,* **37**, 573-578 (2004).

[129] J. Tao and S. Shivkumar, *Mater Lett,* **61**, 2325-2328 (2007).

[130] A. Koski, K. Yim, and S. Shivkumar, *Mater Lett,* **58**, 493-497 (2004).

[131] A. Frenot and I.S. Chronakis, *Curr. Opin. Colloid Interface Sci.,* **8**, 64-75 (2003).

[132] C. Mit-uppatham, M. Nithitanakul, and P. Supaphol, *Macromol. Chem. Phys.,* **205**, 2327-2338 (2004).

[133] E. Zussman, D. Rittel, and A. Yarin, *Appl. Phys. Lett.,* **82**, 3958-3960 (2003).

[134] X. Zong, S. Ran, D. Fang, B.S. Hsiao, and B. Chu, *Polymer,* **44**, 4959-4967 (2003).

[135] S. Zarkoob, R. Eby, D.H. Reneker, S.D. Hudson, D. Ertley, and W.W. Adams, *Polymer,* **45**, 3973-3977 (2004).

[136] F. Ko, Y. Gogotsi, A. Ali, N. Naguib, H. Ye, G. Yang, C. Li, and P. Willis, *Adv Mater,* **15**, 1161-1165 (2003).

[137] Y. Dror, W. Salalha, R.L. Khalfin, Y. Cohen, A.L. Yarin, and E. Zussman, *Langmuir,* **19**, 7012-7020 (2003).

[138] W. Salalha, Y. Dror, R.L. Khalfin, Y. Cohen, A.L. Yarin, and E. Zussman, *Langmuir,* **20**, 9852-9855 (2004).

PORPHYRIN IONIC SELF-ASSEMBLY

On the nano-scale, the ability to produce various geometric shapes allows for the expression and exploitation of specific material properties not seen in the corresponding bulk-scale. In this respect, the self-assembly of porphyrin systems into different nano-scale geometric structures has been an intense area of research. Using the freebase and diacid forms of tetrakis (4-sulfonatophenyl) porphine, and by varying the ionic strength of aqueous solutions used, single and bundled nanorods can be produced [1]. In other instances a mixture of tetrakis (4-sulfonatophenyl) porphine and Sn (IV) tetrakis (4-pyridyl) porphyrin may be used to produce a mixture of nanotubes and nanorods [2]. These approaches employ non-covalent interactions to produce the porphyrin-based nanostructures and have been used by various researchers to form porphyrin nanotubes or nanorods [3]. In the current work, the porphyrin self-assembly was followed by studying the absorption properties of porphyrin aggregates with respect to time, concentration and solvent in the 250 – 1100 nm range. During the aggregation process, there are changes in the intensity of the main absorption band while several new absorption bands appear in the spectra either at lower or higher wavelengths and an intense change in the colour of the solution can be observed. Understanding the aggregation of porphyrins by self-assembly as well as factors affecting this process is essential for their successful implementation in nanodevices.

3.1. Ionic self-assembly of porphyrin nanorods into nanostructures

This work is based on the synthesis of porphyrin nanorods by ionic self-assembly as well as the effect of time, concentration and solvent. This work has been published in the paper:

Synthesis and characterization of porphyrin nanotubes-rods for solar radiation harvesting and solar cells (N. Mongwaketsi, S. Khamlich, B. Klumperman, R. Sparrow, M. Maaza. Physica B 407 (2012) 1615–1619).

3.1.1. Introduction

In natural systems the porphyrins are self-assembled into nanoscale structures that perform light-harvesting and energy and electron transfer functions. A number of artificial porphyrins have the ability to self-assemble intofibers, nanorods, or stripes [1,4,5], with interesting optical and electronic properties [6]. However, there are instances where porphyrin nanosheets or fractures are produced and such nanostructures are in less useful forms [7,8]. Studies are now focused on producing well-defined and robust porphyrin nanostructures. This study is based on preparing well-structured porphyrin nanorods by ionic self-assembly [9] of two oppositely charged porphyrins in aqueous solution. Molecular recognition between the arrangements of opposite charges and hydrogen bond donors and acceptors on the porphyrins contributes to the ionic self-assembly process. During self-assembly there are also electrostatic forces, van der Waals, hydrogen bonding, axial coordination, and other weak intermolecular interactions between the porphyrins. These lead to the formation of porphyrin aggregates and enhance the structural stability of the resulting nanostructures [8].

3.1.2. Materials and methods

Sample preparation

The two porphyrin monomers *meso-tetrakis* (4-phenylsulfonicacid) porphyrin (H_2TPPS_4) dihydrochloride and Sn (IV) *tetrakis* (4-pyridyl) porphyrin dichloride $SnTPyPCl_2$ were purchased from Frontier scientific and used without further purification. The structures of the two porphyrins are shown in Figure 5. The Sn-(IV) center is comprised of (X, X') Cl-, OH-, H_2O) bound above and below the porphyrin plane. At pH 2, X=OH^- and X'=H_2O (net charge+5) or X=X'=OH^- (net charge +4). Hydrochloric acid (HCl) (98 %), phosphoric acid (H_3PO_4) (10 %), nitric acid (HNO_3) (5.5 %) and oxalic acid ($H_2C_2O_4$) (3 %) were purchased from Sigma-Aldrich and prepared with deionized water.

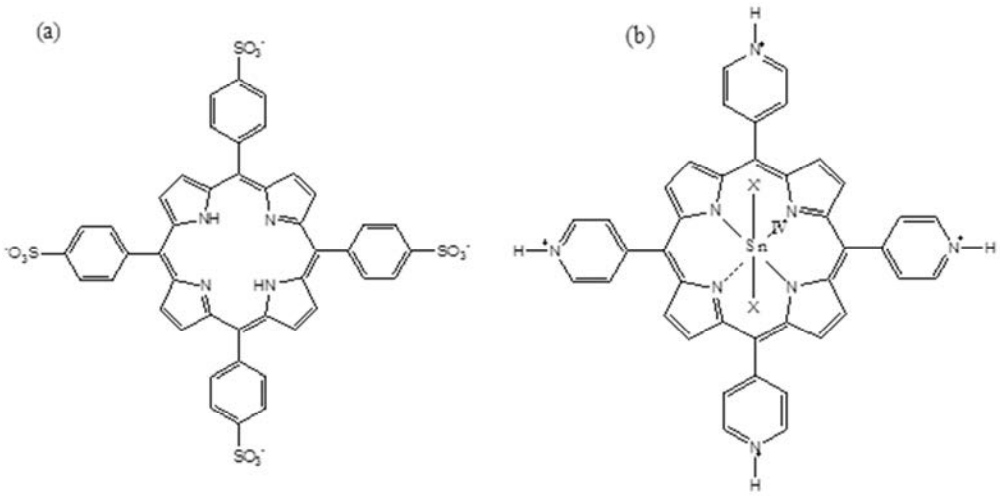

Figure 5. The structure of the porphyrins precursors used for producing nanorods (a) $[H_2TPPS_4]^{2-}$ and (b) $[Sn\ (X)(X')TPyP]^{4+/5+}$.

The two porphyrin solutions (10.5 µM $H_4TPPS_4^{2-}$, 0.02 M HCl) and (3.5 µM $SnTPyP^{2+}$, H_2O) were prepared. Equal volumes of the two aqueous solutions were mixed, obtaining a final solution of pH 2 which was adjusted by adding 0.2 M HCl. The solution was thoroughly homogenized, producing a yellowish-green solution with $H_4TPPS_4^{2-}$, $SnTPyP^{2+}$ and HCl concentrations of 5.25 µM, 1.75 µM, and 10 µM respectively [10].The solution was then stored in the dark at room temperature for 72 hours, until a greenish precipitate was formed. This was followed by spectroscopic and microscopic investigations to confirm formation of the porphyrin nanorods.

3.1.3. Time, concentration and solvent effects on ionic self-assembly of porphyrins

The time dependency on self-assembly of porphyrin monomers was monitored by measuring the UV-VIS absorbance every 30 minutes for a period of 21.5 hour.

In order to investigate the effect of concentration on porphyrin monomer self-assembly, the same procedure as above was followed but in this instance the concentrations of the porphyrin precursor solutions were increased as follows:

- ✓ (21 µM $H_4TPPS_4^{2-}$, 0.02M HCl : 7 µM $SnTPyP^{2+}$, H_2O)
- ✓ (52.5 µM $H_4TPPS_4^{2-}$, 0.02 M HCl : 17.5 µM $SnTPyP^{2+}$, H_2O)

The effect of different solvents on the porphyrin self-assembly was also investigated using a procedure slightly modified from the one described previously. HNO_3, H_2SO_4, H_3PO_4 and $H_2C_2O_4$ with lower solution concentrations were used instead of HCl as follows:

- ✓ (10.5 µM $H_4TPPS_4^{2-}$, 0.01 M HNO_3 : 3.5 µM $SnTPyP^{2+}$, H_2O)
- ✓ (10.5 µM $H_4TPPS_4^{2-}$, 0.01 M H_2SO_4 : 3.5 µM $SnTPyP^{2+}$, H_2O)
- ✓ (10.5 µM $H_4TPPS_4^{2-}$, 0.01 M H_3PO_4 : 3.5 µM $SnTPyP^{2+}$, H_2O)
- ✓ (10.5 µM $H_4TPPS_4^{2-}$, 0.01 M $H_2C_2O_4$: 3.5 µM $SnTPyP^{2+}$, H_2O)

3.1.4. Porphyrin nanorods characterization techniques

The Zeiss 912-Omega transmission electron microscope (TEM) equipped with an in-line mega filter for composition selective transmission imaging and quantitative electron diffraction was used for morphological characterization of nanostructures. Electronic absorption spectra of the porphyrin nanorods solutions were measured using UV-VIS spectroscopy (CECIL 2021 UV-VIS spectrophotometer, scanned from 250 nm – 1100 nm, using scan rate of 200 nm / minute, slit width of 0.2 nm, path length of 10 mm). Optical reflectance spectra in the wavelength range 400 – 1000 nm were obtained with UV-visible Cary 1E system spectrophotometer. The wavelength range was 200 - 900 nm and a sphere diameter of 73 mm. The angle of incidence was zero degrees and the ratio of the aperture area to the total surface area was less than 9 %. Fluorescence excitation spectra were measured using a Shimadzu RF-5301PC fluorescence spectrophotometer with a 150 W xenon lamp.

3.1.5. Results and discussions

3.1.5.1. Porphyrin nanorods characterization

The formation of porphyrin nanostructures in solution was confirmed by TEM. The TEM image in Figure 6 show solid cylindrical shapes with diameters between 20 nm and 60 nm, and lengths as small as 400 nm. The UV-VIS absorbance spectra of the porphyrin precursors and porphyrin nanorods were recorded and are shown in Figure 7. The measured solutions concentrations for $H_4TPPS_4^{2-}$ and $SnTPyP^{2+}$ were 5.25 µM and 1.75 µM respectively.

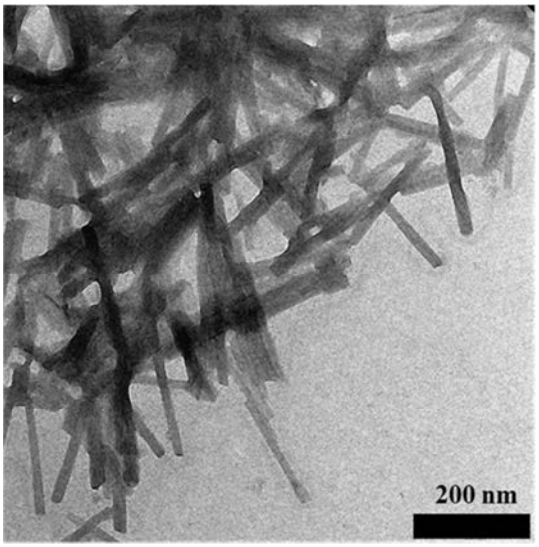

Figure 6. TEM micrograph of synthesized porphyrin nanorods in aqueous solution.

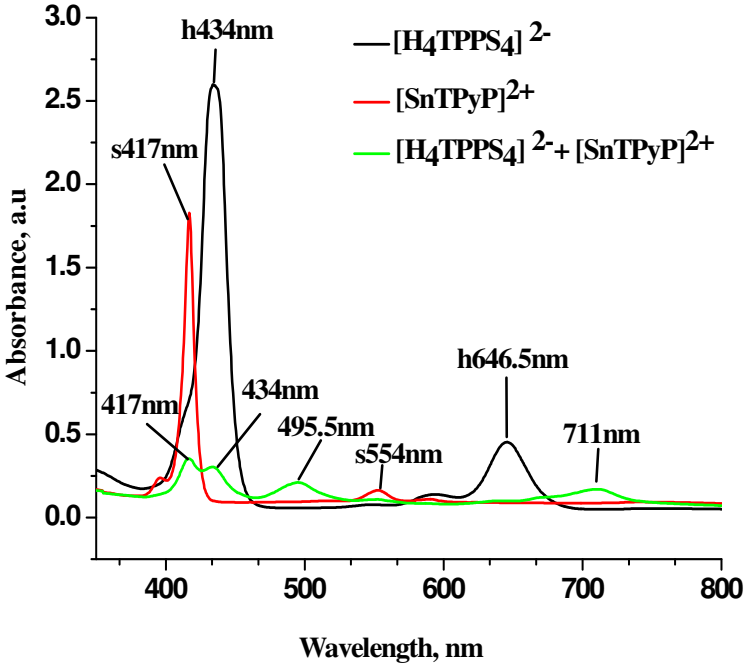

Figure 7. The UV-VIS absorbance spectra of the precursors and porphyrin nanorods formed after mixing of the precursors. Peak labels with the letter 's' are for the $SnTPyP^{2+}$ monomer, the values with an 'h' are for the $H_4TPPS_4^{2-}$ monomer, and the remaining values are for the porphyrin nanorods formed.

The UV-VIS absorption bands of the porphyrin result from electronic transitions from ground state (S_0) to the two lowest singlet-excited states S_1 (Q state) and S_2 (S state) [11].The UV-VIS spectra of the precursors and the resulting nanorods in solution show a decrease in the main absorbance peaks of the precursors and the several peaks identified in the spectrum for the nanorods — 417, 434.5, 495.5, 711 and 974 nm. This may be explained by formation of J-aggregates resulting from the strong coupling of the transition dipoles of individual porphyrin molecules, leading to the formation of new, delocalized excitonic states in the system [1]. The reduction of absorption with increasing particle size is caused by specific surface reduction with growing particle size and this effect is readily observed in wavelength regions where molecules have high absorption strength. The formation of hetero-aggregates, as in the present study, is usually characterized by decreased absorbance intensities of all bands with band broadening compared with precursor molecules [12], and by observation of the movement of the J-aggregate band to longer wavelength compared with that of homo-aggregates of $H_4TPPS_4^{2-}$. Exciton theory states that when molecules lie in a head-to-tail arrangement (J-aggregation) the allowed state is lower in energy and this will result in a red-shift relative to the monomer [13]. The Soret band of $[H_4TPPS_4]^{2-}$ is red-shifted upon aggregation (J-aggregate) due to the planar porphyrin molecules stacking in an arrangement where individual porphyrin units are not positioned directly one on top of the other. The porphyrin nanorods spectrum showed two additional Q-bands at longer-wavelength region as compared to the precursor spectra which showed single absorbance peak in the region. One of the key factors in the design of artificial light harvesting systems is the absorption in the UV-VIS and near-infrared wavelengths and the fact that porphyrin nanorods exhibit additional absorption bands in that region suggests that they have the potential of being exploited as artificial solar harvesters.

3.1.5.2.Time effect on porphyrin self-assembly (UV-VIS spectroscopy)

UV-VIS spectroscopy was used to follow the growth dynamics after mixing the porphyrin precursors solutions. The UV-VIS absorption was measured in 30 minutes time intervals until the1290 th min. The UV-VIS absorption spectra revealed that with time the porphyrins begin to aggregate and the absorption bands generally broadened and red-shifted. Over time the there was no significant change in transparency of the solutions.

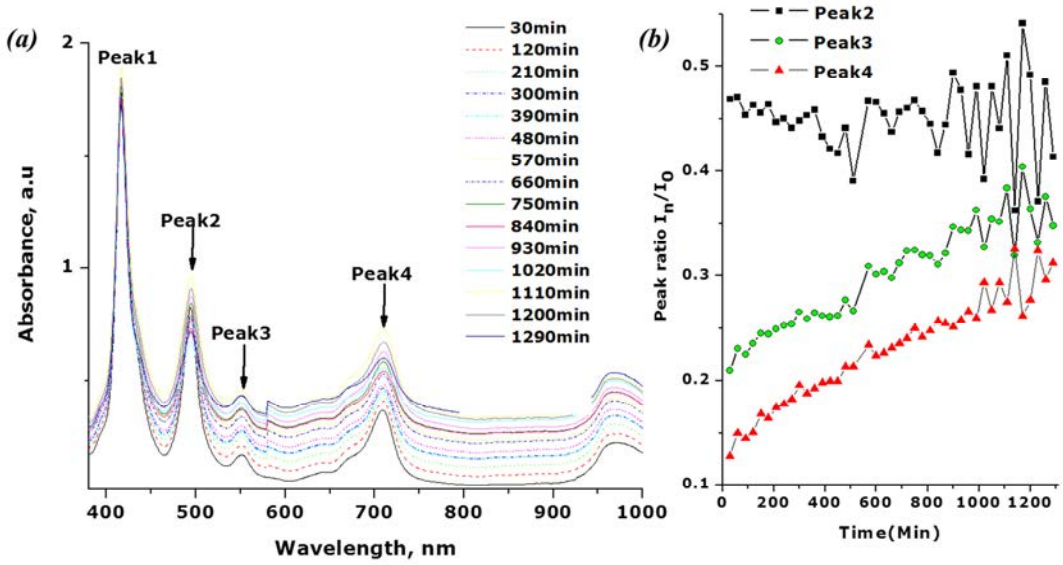

Figure 8. (a) The UV-VIS absorbance of $H_4TPPS_4^{2-}$ and $SnTPyP^{2+}$ monomer solutions measured after mixing for Time 30 min-Time 1290 min. (b) Graphs showing the change in the peak ratio related to the time of porphyrin nanorods growth.

Figure 8 (a) shows changes observed for the absorbance peaks at 495.5, 554 and 711 nm, with small shifts and broadening to longer wavelengths. This is an indication that there was regular growth in the dye layers [14]. Figure 8 (b) shows peak ratio between the peaks 1:2:3:4 with peak1 used as the reference due to its constant absorbance. Both peaks 3 and 4 show a similar trend from 30 minutes until the 16.6 hour. Whereas for peak 2 it was assumed that the porphyrins aggregate reach a steady point and then regain aggregation at some further point in time. The broadening of the J-aggregate bands is an indication that a large number of porphyrin molecules played a part in the formation of aggregates. It is thought that the driving force for rod formation is electrostatic interaction between negative sulfonate groups and the positive core of the adjacent molecules [15,16]. While there are several proposed structures for the rods that are consistent with this ionic self-assembly pattern [15], there is no general agreement on exactly how the molecules form the observed rods.

3.1.5.3. Concentration effect on porphyrin self-assembly (UV-VIS spectroscopy)

The effect of increasing concentrations of porphyrin monomers on self-assembly was investigated. The UV-VIS spectra shown in Figure 9 follow the self-assembly process as the porphyrin concentration increases at a constant pH = 2. An increase in the porphyrin concentration resulted in a decrease and slight broadening of the peaks at 418, 594 and 646 nm. The broadening of the bands indicates the presence of protonated state of a porphyrin macrocycle. A shift of the Soret band to lower wavelengths (433 - 418 nm) was observed and there was no appearance or disappearance of any of the bands. This may be attributed to insignificant change in the symmetry of the molecule upon macrocycle protonation. There was no shift of the Q-bands at 646 nm as the concentration was increased, implying that there was a constant gap of the energy level of the Q-bands during electronic transitions. Increased porphyrin concentrations usually result in self-assembly into rod-like nanostructures and with further increase in concentration, the rod-like shape is maintained but tend to be shorter [1,17]. A decrease in the rods length with increasing concentration was reported previously [17, 18] and concentration of porphyrin and storage time of the acidic solution could influence the length and not the diameter of the aggregates [19].

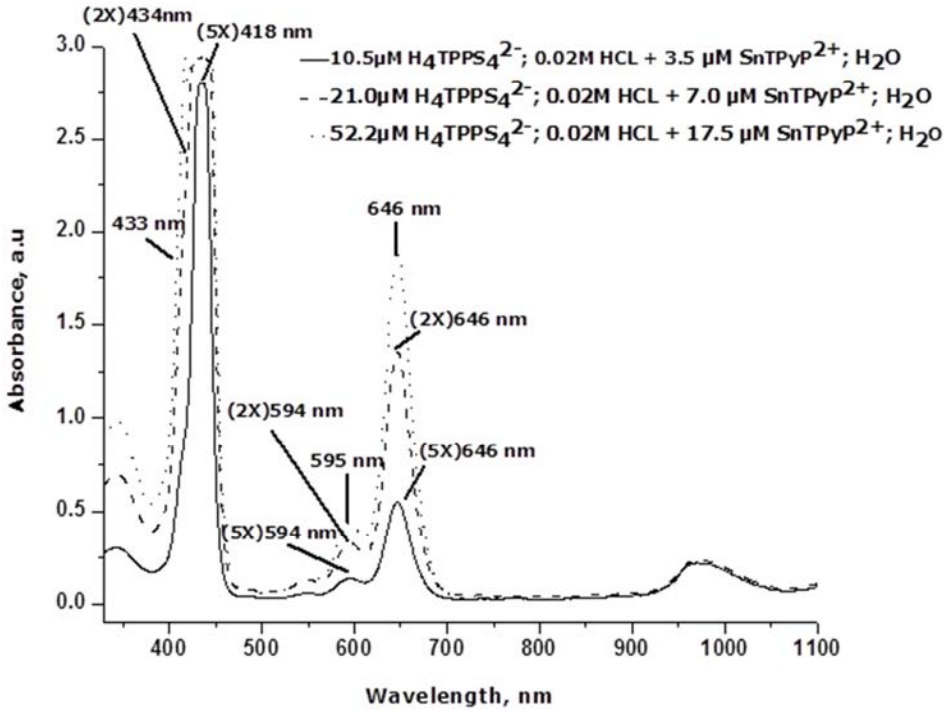

Figure 9. The UV-VIS spectra of porphyrin nanorods solutions of different concentrations. Peak labels with '2X' and 5X are for the doubled and five times concentrated mixtures.

3.1.5.4.Solvent effect on porphyrin self-assembly (UV-VIS spectroscopy)

The UV-VIS spectra for all solvents used except for HNO_3, Figure 10; showed intense narrow absorbance peaks in the near UV-region (400 - 460 nm) together with three weaker Q-bands at ~ 495, 552 and 709 nm. It was noteworthy from the HNO_3 UV-VIS spectrum that the Soret and the Q bands appeared broaden and exhibited red shifts. The Soret band was red shifted whereas the Q-bands remained similar as in other solvent media. This may be attributed to stronger exciton coupling causing a shift of the Soret band during porphyrin molecules aggregation. The observed band shifts and broadening can be attributed mainly to changes in the solvent polarizability and it is possible that the band shifts may be reflecting a combination of solvent effects and a number of dimerization processes. The absorbance intensity for the normal solvent (HCl) was the lowest of all the solvents used with two bands at 416 and 433 nm and weaker Q-bands at 495, 552 and 709 nm. The increase in absorption intensity of other solvents compared to the HCl medium may be caused by the formation of the aggregates with ordered structures in the system.

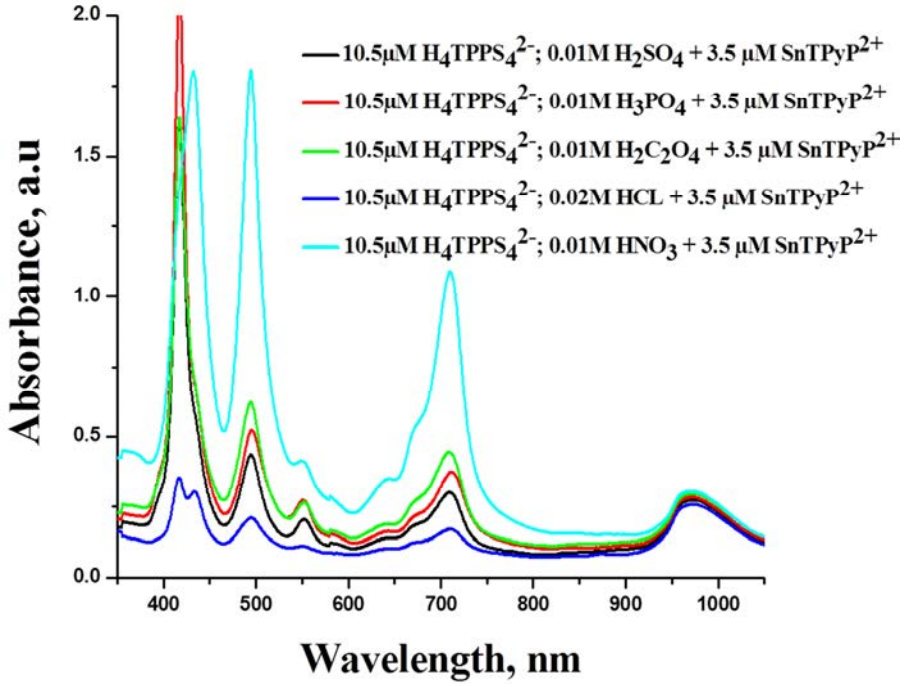

Figure 10. The UV-VIS absorbance spectra of porphyrin nanorods formed after mixing of the precursors in different solvents.

For all the solvents used porphyrins were able to self-assemble into rod-like nanostructures with differences in diameters and lengths. There were no other morphologies seen in the TEM images. TEM, Figure 11 (a) - (d), revealed that; the average diameter of nanorods formed using H_2SO_4 was 36.40 nm, 31.57 nm for H_3PO_4 , 29.8 nm for $H_2C_2O_4$ and 27.03 nm for HNO_3 solvent. The majority of the nanorods in H_2SO_4 as the solvent were longer as compared to nanorods obtained in other solvents. These were followed by those of H_3PO_4, $H_2C_2O_4$ and HNO_3 in order of decrease in lengths respectively. TEM also showed that the use of H_3PO_4 as a solvent produced highly agglomerated nanorods as compared to those produced using the other solvents; see Figure 11 (b). For $H_2C_2O_4$ solvent, most of the nanorods produced appeared to be broken, Figure 11 (c).Any sufficient stresses experienced by the nanorods may have led to breakage at the mechanically weak part of the array.

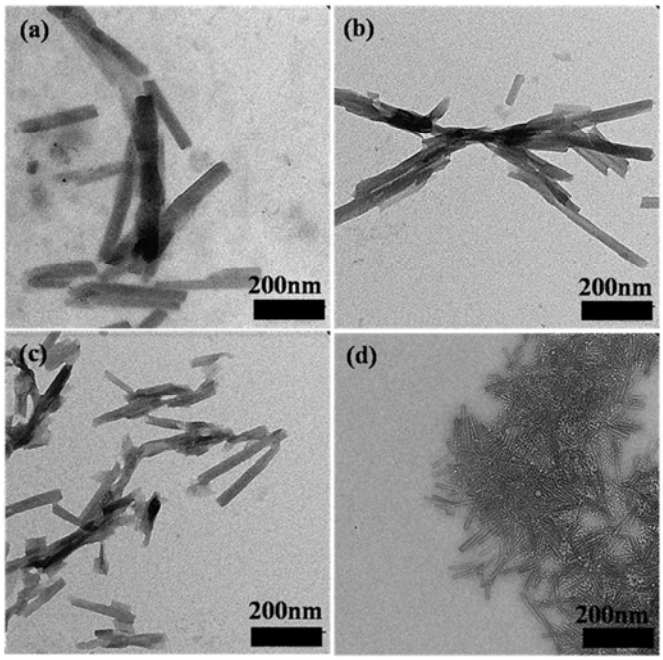

Figure 11. TEM micrographs of the porphyrin nanostructures solutions drop-dried on a copper grid. Different acids were used as solvents; (a) H_2SO_4, (b) H_3PO_4 (c) $H_2C_2O_4$ and (d) HNO_3.

3.1.5.5. Solvent effect on porphyrin self-assembly (UV-VIS reflectance spectroscopy)

Diffuse reflectance spectra of aqueous porphyrins were recorded in wavelength range from 300 to 800 nm. Reflectance data are usually expressed in terms of percent reflectance which is analogous to percent transmission in absorption spectroscopy.The spectra recorded for the reflectance measurements of porphyrin nanorods prepared under different solvent conditions are shown in Figure 12. The bands at ~ 490 – 500 nm, as depicted by the reflectance spectra, are typical of the Soret band of the UV-VIS absorption spectra of porphyrin in homogenous solutions. These broad bands at ~490 – 500 nm are attributed to the formation of porphyrin aggregates in solutions and the low intensity of the Q-bands may possibly result from the effect of light scattering. The reflectance measurements of the porphyrin nanorods solutions, showed that the porphyrin nanorods have very low reflectance, with a maximum at λ = 495 nm and 0.16 % reflectance for $H_2C_2O_4$, λ = 498 nm and 0.15 % reflectance for H_2SO_4, λ = 488 nm and 0.1 % reflectance for HCL and λ = 495 nm and 0.07 % reflectance for H_3PO_4.

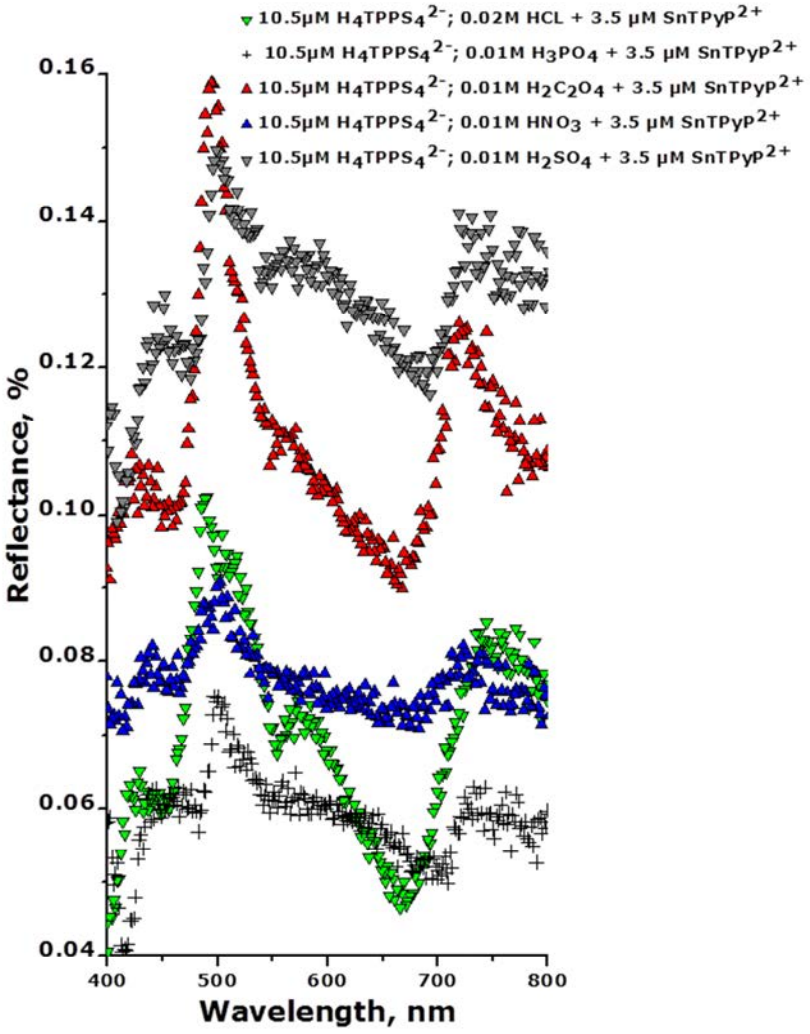

Figure 12. The total reflectance spectra of porphyrin nanorods prepared from different solvents on glass substrate.

3.2.Single molecule spectroscopic investigation on self-assembly of porphyrins

3.2.1. Introduction

Single molecule spectroscopy (SMS) technique was used to investigate further porphyrin self-assembled molecules. This technique allows individual members of a population to be probed; thereby yielding more direct information regarding the distribution of molecular and kinetic properties [20] and this also provides information about dynamical interaction between porphyrin molecules and the host matrix. Most of the single molecules investigated belong to a class of conjugated aromatic hydrocarbons. These compounds are best for SMS

characterization since they have a strongly allowed transition in their absorption spectra and high fluorescence quantum yields [21].

The time-resolved fluorescence of porphyrin aggregates were studied in order to obtain information regarding the photophysical processes in excited states of the aggregates. The lifetime of the excited state is the average time that the molecules spend in the excited state before returning to ground state .The lifetime determines the time available for the fluorophore to interact by energy transfer processes or diffusion with its environment. The fluorescence anisotropy of the aggregates was also studied, and for this measurement the fluorophores specifically absorb photons whose electric vectors are aligned parallel to the transition moment of the fluorophore. Data form these measurements can provide information on the orientation of a fluorophore which is one of the important properties for energy transfer processes.

3.2.2. Materials and methods

Sample preparation

The porphyrin nanorods solution (10.5 µM $H_4TPPS_4^{2-}$, 0.02 M HCl and 3.5 µM $SnTPyP^{2+}$, H_2O) investigated was prepared as described in Section 3.1.2. To prepare samples for SMS analysis, 5 µL of porphyrin nanorods solution prepared was mixed with (45 µL) 1% poly vinyl alcohol (PVA). A unidirectional oriented film with porphyrin nanorods was prepared using a vertical spin-coating technique. This was undertaken to immobilize the molecules in dense PVA to prevent translational diffusion during the 100 ms exposure time. If the molecules were not immobilized they could diffuse several microns during this time and not be seen in the image. Fluorescence anisotropy decays of individual molecules and fluorescence lifetime were measured on porphyrin aggregates fixed in a PVA matrix. Stability of the emission from single molecules was monitored by recording the images generated during the continuous irradiation of the sample at a fixed excitation wavelength of 640 nm.

3.2.3. Characterization technique

Fluorescence and fluorescence lifetime measurements

Fluorescence emission spectra were recorded on an in-house customized instrument. The microscope configuration consisted of: an inverted Olympus IX70 microscope, a Triax 320 imaging spectrograph with a back illuminated liquid nitrogen cooled charge coupled device (CCD) camera (Spectrum One, JobinYvon, 2048 x 512 pixels, pixel size 13,5 x 13,5 μm) and a picosecond-pulse laser diode module (PicoQuant LDH-D-C-640, 640 nm, lin. polar) as an excitation source. The CCD was an integrating detector that measured the total intensity during the data collection time. Objects were enlarged with an objective Olympus 100 x, NA of 1.35, UMPLANFL infinity-0, and samples excited with 640 nm light by total reflection. The microscope was equipped with an Olympus filter cube (Olympus, Japan) containing a Raman emitter RS 664 LP (679.3 - 1497.7 nm), an HC-Laser Cleanup MaxDiode 640-8 (Semrock, Germany). Two single photon counting avalanche photodiodes (Perkin Elmer, SPCM-AQR-16) were attached to the side exit of the Triax-monochromator for fluorescence correlation spectroscopy and fluorescence lifetime measurements. The experimental conditions for SMS were: 20 MHz frequency, 5 mm slit, the exposition time for transmission was ~ 40 ms, and for fluorescence images ~ 7000 ms. Magnification 100 x (1.35 NA, oil immersion, UplanApo), 0.7 T magnetic field.

3.2.4. Results and discussions

3.2.4.1. Porphyrin single molecular fluorescence

Single molecule fluorescence spectra were measured for six individual porphyrin molecules fixed in a PVA matrix. The porphyrin solution investigated was a mixture of $H_4TPPS_4^{2-}$ and $SnTPyP^{2+}$ aqueous solutions. This was also to investigate the excited-state dynamics in self-assembled porphyrins. The individual fluorescence excitation spectra were acquired by analysis of signals coming from the single molecules as a function of the laser frequency. The single molecule fluorescence spectra of the porphyrin nanorods in Figure 13 exhibited a distinctive peak around 720 nm which may be attributed to the fluorescence of the porphyrins

J-aggregates [22]. An insert in Figure 13 shows the fluorescence from individual porphyrin molecules.

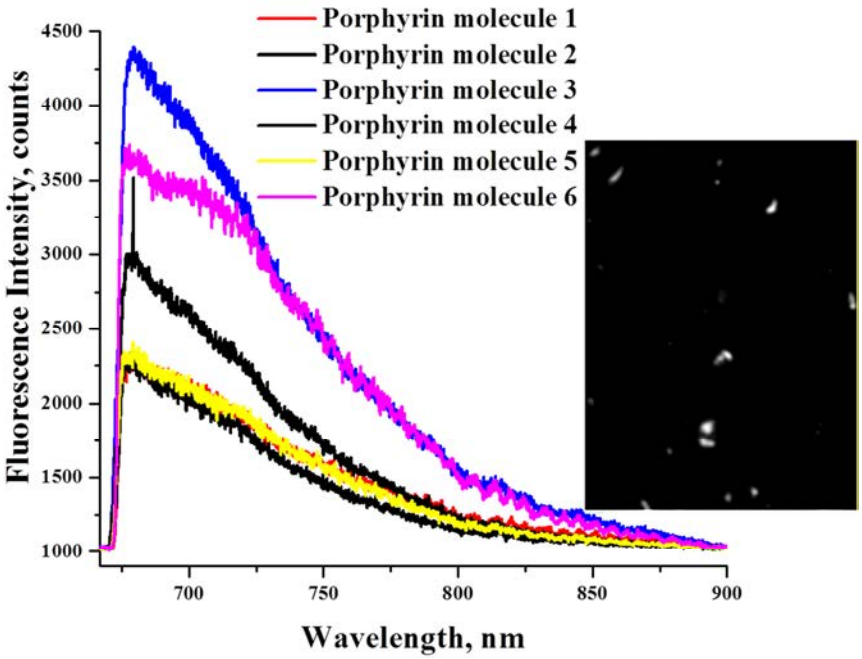

Figure 13. Figure showing the fluorescence spectra of six individual porphyrin molecules fixed in the PVA matrix.

3.2.4.2.Time-resolved fluorescence anisotropy of porphyrin aggregates

To further understand the nature of the aggregates formed in the interaction of the two porphyrin monomers, time-resolved fluorescence anisotropy studies were carried out. This technique was employed to elucidate dynamic information about the porphyrin aggregates in a confined environment [23].The intrinsic anisotropy r_0 is measured by embedding the fluorophore in a dense medium. When the fluorophores can freely change their orientation before re-emitting the photons, the degree of polarization of the emitted light will be reduced. The extent of reducing autocorrelation in the polarization of the incident and emitted light is dependent on the rotational lifetime compared to the fluorescence lifetime (τ), denoted tau in Figure 14.

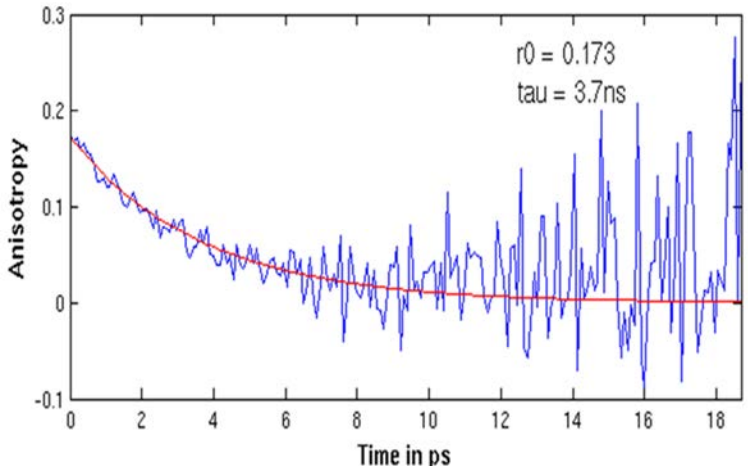

Figure 14. The time-resolved fluorescence anisotropy decay curves. Blue line represents calculated anisotropy decay and red is fit of the decay.

Table 1. The time-resolved fluorescence anisotropy of porphyrin aggregates.

Aggregate	Anisotropy decay time, tau (ns)	Intrinsic Anisotropy (r0)
1	3.7	0.173
2	2.3	0.153
3	0.5	0.149

The fluorescence anisotropy decay times of the porphyrin aggregates studied were in the range 0.5 – 3.7 ns. The anisotropy decay time of 0.5 nm which is the fastest is thought to originate from self-assembled porphyrins and 3.7 nm time may be due to fluorescence from porphyrin individual molecules [24]. The time dependency of the anisotropy is most likely as a result of energy transfer between porphyrin molecules and among different aggregates in the polymer matrix.

In order to obtain information on time the molecules stayed in excited states before emitting photons, the fluorescence lifetime of porphyrin aggregates were measured and the data is summarised in Table 2.

Table 2. The fluorescence lifetime data for the porphyrin aggregates.

Porphyrin aggregates	Fluorescence lifetime (ns)
1	0.7
2	2.97
3	3.27
4	2.98
5	2.85
6	2.45

The value of chlorophyll fluorescence lifetime found in a previous study was 4.9 ± 2 ns [25]. The porphyrin aggregate studied exhibited shorter fluorescence lifetime of 0.7 ns with the longest lifetime being 3.27 ns. If the lifetime of the excited state is longer, the orientations of the excited molecules are to some extent randomized. The studied porphyrins may experience less of this effect because porphyrin aggregates have short-lived fluorescence lifetime [24] and are in this instance self-assembled. The porphyrin aggregates shorter fluorescence lifetimes may also be because of larger dipole moment surrounding molecules which in turn increase the efficiency of energy transfer. These results are promising in terms of artificial light harvesting applications, since in natural systems, fluorescence lifetime of aggregated chlorophylls are shorter than those of monomeric chlorophylls because of energy transfer within the chlorophyll aggregates [26].

3.3. Conclusion

The production of porphyrin nanorods by ionic self-assembly was successfully executed.The reason for the porphyrins assembling into a rod shape rather than any other shape is probably due to the specific intermolecular interactions that occur between the individual porphyrin molecules. The Soret band of the studied porphyrins nanorods appeared in the area of 417 and 435 and weaker Q-bands lie in the region from 495.5-700 nm. This provides a broad absorbance spectrum that is desirable in producing light harvesting systems. Optical investigations on the produced nanorods were conducted as well as the effect of time,

concentration and solvent on the self-assembly of porphyrins. Similar or improved optical and morphological results were obtained with 0.2 % reflectance indicating the potential use of the studied porphyrin-based nanorods as light harvesters. The fluorescence measurement using single molecule spectroscopy showed that porphyrin single molecules exhibited shorter fluorescence lifetimes which are associated with energy transfer mechanism, and this implies that the nanorods produced by self-assembly between $H_4TPPS_4^{2-}$ and $SnTPyP^{2+}$ may serve as electron donors in artificial light harvesting systems.

The handling of porphyrin nanorods in aqueous media and lack of precise arrangement are some of the limiting factors for photonics applications. In order to study further the porphyrin nanorods as potential artificial light harvesting component their incorporation into polymer matrices is important. We therefore attempted to obtain porphyrin nanorods embedded in polymer matrix using latex technology, electrospinning and self-assembly on the surface of a membrane and these approaches are discussed in the next chapter.

.

3.4. References

[1] A.D. Schwab, D.E. Smith, C.S. Rich, E.R. Young, W.F. Smith, and J.C. de Paula, *J. Phys. Chem. B,* **107**, 11339-11345 (2003).

[2] Z. Wang, C.J. Medforth, and J.A. Shelnutt, *J. Am. Chem. Soc.,* **126**, 15954-15955 (2004).

[3] F. Dini, E. Martinelli, G. Pomarico, R. Paolesse, D. Monti, D. Filippini, A. D'Amico, I. Lundström, and C.D. Natale, *Nanotechnology,* **20**, 055502 (2009).

[4] R. Rotomskis, R. Augulis, V. Snitka, R. Valiokas, and B. Liedberg, *J. Phys. Chem. B,* **108**, 2833-2838 (2004).

[5] U. Siggel, U. Bindig, C. Endisch, T. Komatsu, E. Tsuchida, J. Voigt, and J.H. Fuhrhop, *Berich Bunsen Gesell,* **100**, 2070-2075 (1996).

[6] T.J. Marks, *Science,* **227**, 881-889 (1985).

[7] X. Gong, T. Milic, C. Xu, J.D. Batteas, and C.M. Drain, *J. Am. Chem. Soc.,* **124**, 14290-14291 (2002).

[8] N. Micali, A. Romeo, R. Lauceri, R. Purrello, F. Mallamace, and L.M. Scolaro, *J. Phys. Chem. B,* **104**, 9416-9420 (2000).

[9] C.F.J. Faul and M. Antonietti, *Adv Mater,* **15**, 673-683 (2003).

[10] R. Franco, J.L. Jacobsen, H. Wang, Z. Wang, K. István, N.E. Schore, Y. Song, C.J. Medforth, and J.A. Shelnutt, *Phys. Chem. Chem. Phys.,* **12**, 4072-4077 (2010).

[11] X. Sun, G. Chen, and J. Zhang, *Dyes and Pigments,* **76**, 499-501 (2008).

[12] R.C. George, G.O. Egharevba, and T. Nyokong, *Polyhedron,* **29**, 1469-1474 (2010).

[13] S.M. Andrade, R. Teixeira, S. Costa, and A.J.F.N. Sobral, *Biophys. Chem.,* **133**, 1-10 (2008).

[14] E. Rousseau, M.M. Koetse, M. Van der Auweraer, and F.C. De Schryver, *Photochem. Photobiol. Sci.,* **1**, 395-406 (2002).

[15] C.J. Medforth, Z. Wang, K.E. Martin, Y. Song, J.L. Jacobsen, and J.A. Shelnutt, *Chem.Commun.,* 7261-7277 (2009).

[16] S. Vlaming, R. Augulis, M. Stuart, J. Knoester, and P. Van Loosdrecht,*J. Phys. Chem. B,* **113**, 2273-2283 (2009).

[17] N. Micali, V. Villari, M.A. Castriciano, A. Romeo, and L.M. Scolaro, *J. Phys. Chem. B,* **110**, 8289-8295 (2006).

[18] S. Gandini, E. Gelamo, R. Itri, and M. Tabak, *Biophys. J.,* **85**, 1259-1268 (2003).

[19] M. Wei and Y. Lu, *Synth. Met.,* **159**, 1061-1066 (2009).

[20] C. Eggeling, J.R. Fries, L. Brand, R. Ganther, and C.A.M. Seidel, *Proc. Natl. Acad. Sci.,* **95**, 1556 (1998).

[21] A. Starukhin, A. Shulga, J. Sepiol, R. Kolos, A. Renn, and U.P. Wild, *Simol,* **2**, 203-206 (2001).

[22] L. Kelbauskas, S. Bagdonas, W. Dietel, and R. Rotomskis, *J. Lumin,* **101**, 253-262 (2003).

[23] G. Jia, Z. Feng, C. Wei, J. Zhou, X. Wang, and C. Li, *J. Phys. Chem. B,* **113**, 16237-16245 (2009).

[24] H.K. Seidlitz, H. Schneckenburger, and K. Stettmaier, *J. Photochem. Photobiol.,* **5**, 391-400 (1990).

[25] G.S. Singhal and E. Rabinowitch, *Biophys. J.,* **9**, 586-591 (1969).

[26] G. Picard, G. Munger, R. Leblanc, R. Le Sage, D. Sharma, A. Siemiarczuk, and J. Bolton, *Chem. Phys. Lett.,* **129**, 41-47 (1986).

PORPHYRIN NANORODS-POLYMER COMPOSITES

This chapter is based on the incorporation of porphyrin nanorods in polymer matrices to form composites. Ionic self-assembly of porphyrins into rod-like nanostructures was carried out in aqueous medium and in order to use these nanostructures, their immobilization and incorporation into bulk materials such as polymers is essential. The three explored approaches of incorporating porphyrin nanorods into polymer matrices were:

- ✓ **Self-assembly on the surface of a track-etched membrane.**
- ✓ **Latex blending process.**
- ✓ **Electrospinning process.**

4.1. Introduction

In bacteria and green plants, the photosynthetic light-harvesting antenna complexes and reaction centres are assemblies of bacteriochlorophyll molecules held together by protein scaffolds [1] and such arrangements result in efficient absorption and light energy transfer [2],[3]. Inspired by the precise organization and orientation of the chromophores in natural systems, attention is currently focused on the design of nanometer sized chromophoric assemblies, which may find applications in the field of molecular photonics. However, it is challenging to design multi-component systems with controlled structural arrangement at the molecular level. A lack of precise arrangement may have a negative impact on the construction of an efficient artificial light harvesting system. This chapter explores the possibility of incorporating nanorods into polymer matrices to overcome the limiting factors of applications of these materials in photonic devices. The incorporation of nanoparticles into polymer to produce functional device presents its own set of unique problems [4] but also addresses the challenge of assembling components in a spatially organized manner such as to allow their efficient collaboration in harvesting the light energy in artificial systems [5]. The orientation of dye molecules is of great interest as it displays characteristics of natural antenna systems and also have unique optical and physical properties

[6,7]. A number of methods have been used to incorporate nanoparticles in polymer matrices; these included latex blending technique [8,9], spin coating [10], melt-processing [11-13], electrospinning [14-21] etc. It has been demonstrated by a number of studies [8,22-28] that latex blending can be used successfully to prepare carbon nanotube (CNT)-polymer composites. We explored the latex blending techniques to incorporate porphyrin-based nanorods and attempted to measure the electrical conductivity of the composite. It was not easy to measure the conductivity due to very high resistivity of these composites; this was not surprising as porphyrins do not have current carrying capacity as CNTs. For dispersed CNTs-polymer matrices a percolation threshold of 1 -1.5wt % [13,29] and lower has been reported [30-32]. The purpose of employing electrospinning as one of the experimental techniques to incorporate porphyrin nanorods into a polymer matrix was aimed at obtaining aligned fibres with porphyrin nanorods. This technique was reported as a potential method for aligning nanoparticles with the possibility of nanoparticles being aligned along the streamlines of a jet [33]. Using this technique would also address a challenge of controlling the orientation or alignment of nanorods within the polymer matrix which is also an important aspect for improved properties of the composites. Self-assembly of porphyrin nanorods on the surface of modified track-etched membrane was another explored approach for incorporating the nanorods onto a support. This approach demonstrated how ionic interactions can induce porphyrin self-aggregation on a solid surface. This is of important value in regard to approaches of fabricating nanostructures on solid substrates.

4.2. Porphyrin nanorods-polymer composite by self-assembly on the surface of track-etched membrane

This work is based on the incorporation of porphyrin nanorods on the surface of a track-etched polymer membrane. This membrane has uniform pore structure, excellent porosity and a well characterized surface chemistry. Such a membrane may be used to incorporate nanoparticles to produce devices of interest. This work has been published in the paper:

Ionic self-assembly of porphyrin nanostructures on the surface of charge-altered track-etched membranes (N. Mongwaketsi, G. Ndungu, A. Nechaev, M. Maaza, R. Sparrow. Journal of Porphyrins and Phthalocyanines 14 (2010) 1–6).

4.2.1. Introduction

Track etched membranes were used as matrices for the ionic self-assembly of porphyrin molecules. These membranes have a well-defined structure, and a wide range of controllable pore diameters, porosity and thickness [34,35]. In addition, the physical-chemical properties have been well investigated [34,36,37]. For example, the electrokinetic behavior of track-etched membranes made from poly (ethylene terephthalate) (PET), with pore diameters between 20 – 580 nm, was investigated by Déjardin *et al.* [38]. The adsorption of proteins and water-soluble dyes on such track-etched PET membranes were reported by Khataibe *et al.* [39]. It is interesting to note that the proposed mechanism of adsorption on the surface of the membranes took into account ionic, hydrophobic and hydrophilic interactions [36]; these may be exploited in porphyrin self-assembly onto similar PET substrates.

4.2.2. Materials and Methods

Sample preparation

Membranes with pore diameters of 30 nm – 1 micrometer, and thickness between 10 - 20 micrometers were received from the Flerov Laboratory of the Joint Institute of Nuclear research (Dubna, Russia). The original membranes are negatively charged in water based solutions in the pH range 2.8 – 9 [36,37]. To alter the surface charge, the membranes were modified with water soluble polyethyleneimine (PEI) (M.W. 1800, 99 %, Lancaster). The membranes were modified with 0.01 %, 0.10 %, and 1.00 % (w/w) aqueous solutions of PEI by simply immersing the membranes for 24 hours at ambient conditions. In a typical experiment, the membrane is placed in a Petri dish, and 30 ml of the desired solution is poured over the membrane, this is then left for 24 hours. After which the sample is removed from the solution and air dried under ambient conditions. The membrane bears fixed negative charges at the surface and within pores due to the free carboxyl groups generated by the alkaline hydrolysis of ester bonds during the etching process. These groups will attract the amino groups from the PEI solution in which the membrane was placed. As a result of charge interaction the surface charge of the PET track etched membrane is reversed from negative to positive. Electrokinetic measurements were performed to determine the changes of surface charge on the membranes using the streaming

potential method. This was conducted in a standard cell (Millipore) with built-in silver-chloride electrodes. Measuring the streaming potential (E) through the membrane helps in the characterization of the magnitude of surface charge [38]. The dependence of the potential difference on the pressure drop on the membrane during filtration was measured. The installation for electrokinetic measurements was undertaken according to procedures reported by Berezkin *et al*. [40]. The surface charge was determined by calculating the membrane zeta potential (ζ) using the Helmholtz–Smoluchowski equation:

$$\frac{\Delta \boldsymbol{E}}{\Delta \boldsymbol{P}} = \frac{\boldsymbol{\zeta \varepsilon}}{\boldsymbol{\eta \lambda}} \qquad \textbf{[1]}$$

where ΔP is the pressure drop across the pore channel, η is the solution viscosity, λ is the solution conductivity and ε is the dielectric constant of the electrolyte solution [41].

The methods used to assemble porphyrin nanorods on the membranes included the filtration of pre-assembled nanorods and exposure of PET track etched membranes with different surface charges to porphyrin solutions. A mixture of $H_4TPPS_4^{2-}$ and $SnTPyP^{2+}$ porphyrins was filtered through 0.03 μm, 0.2 μm and 1 μm track-etched membranes. For the membrane exposure to the nanorods solution a successive immersion technique was used. The PEI-modified membrane was inserted in a negatively charged porphyrin nanorods solution for about 24 hours and the UV-visible absorption measured. This was repeated a number of times and the UV-visible absorption measured after each insertion.

4.2.3. Characterization techniques

The SEM, TEM, CECIL 2021 UV-VIS spectrophotometer were used for characterization. The TEM and UV-VIS spectrophotometer descriptions are in detail in Section 3.1.4. The morphology of porphyrin nanorods on the membrane surface was investigated using Leica-LEO Stereoscan S440 and FEI Nova NanoSEM 50 series electron microscopes. Atomic force microscopy (AFM) experiments were conducted and analyzed using a NanomanVeeco AFM. Silicon tips in the range between 12 and 103 N/m, spring constant, ~320 - 355 kHz resonant frequency and 140 -

180 nm length were used to acquire the images in tapping mode. The set point was set to 400 mV for all the scans at the beginning. After engaging the tip, the Z-voltage was slowly tuned down to between 260 - 350 mV. The scan rate was set to 0.9 Hz at the beginning to verify the contact with the surface. For the images, 512 x 512 points were taken. Integral gain was tuned during the scan. The initial value of integral gain was set to 1.

4.2.4. Results and discussion

4.2.4.1. Electro-kinetic properties of the PEI-modified membrane

The results for electro-kinetic measurements on the PEI-modified membrane are illustrated in Figure 15. The electro-kinetic data is similar to results previously reported in the literature[40], and clearly shows the change of the membrane surface charge from negative to positive for all PEI-modified membranes. It must be noted that the PEI layers on the surface of track-etched membrane are stable, and that varying the pH values does not change the electro-kinetic properties of the membranes [34,37].

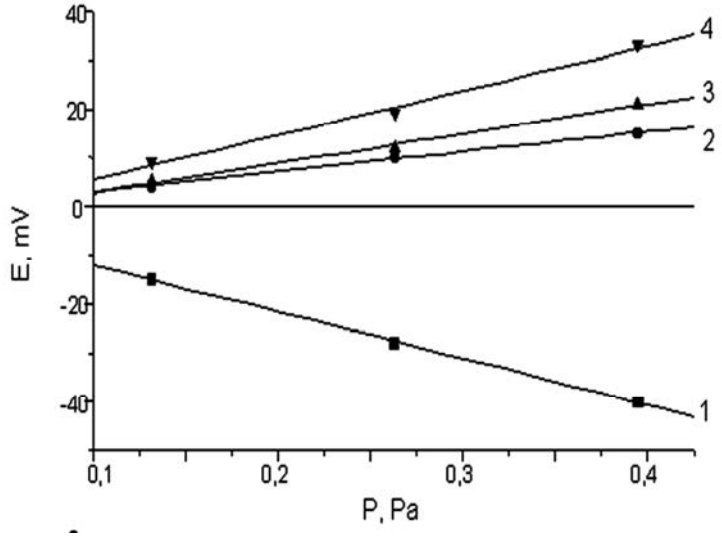

Figure 15. The dependence of streaming potential (E) on pressure difference (P) TM (1: initial TM; 2: TM, modified by 1% water solution of PEI; 3: TM, modified by 0.1% water solution of PEI; 4: TM, modified by 0.01% water solution of PEI). Concentration of KCI = 0.01 M at pH = 6.0.

4.2.4.2. Self-assembly of porphyrin nanorods on track-etched membranes by filtration

SEM was used for morphological characterization of the assembly of porphyrin nanorods onto the surface of a track-etched membrane via filtration. The SEM images showed that some nanorods were randomly distributed onto the surface and others were trapped in the membrane pores irrespective of the pore diameter used, Figure 16. There were a few pores that were not blocked by the nanorods, indicating that the porphyrin nanorods do not completely block the membranes.

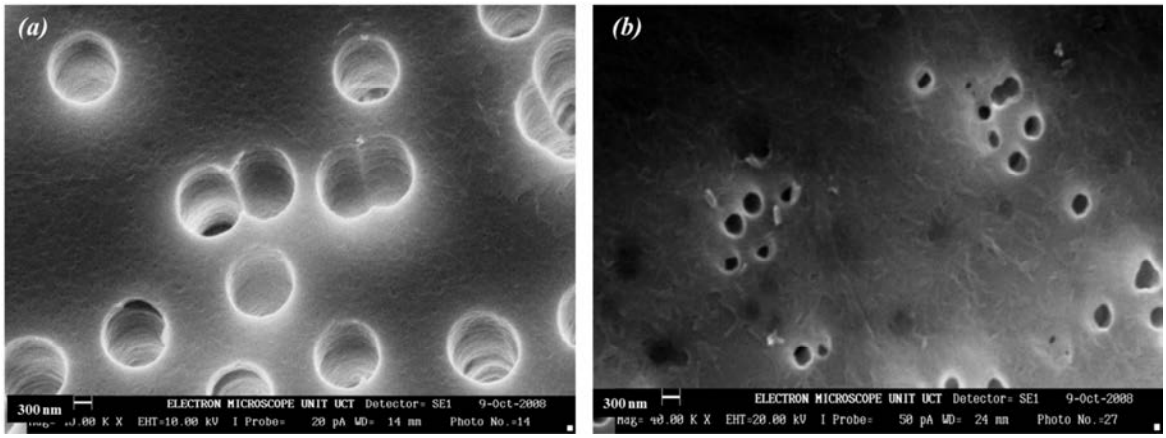

Figure 16. SEM micrographs of (a) pristine track-etched membrane surface, (b) porphyrin nanorods filtered through track-etched membranes.

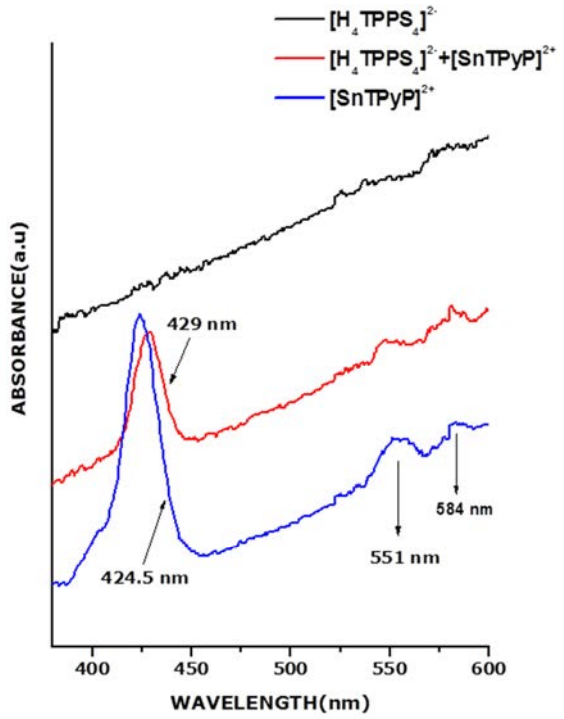

Figure 17. The UV-VIS spectra of various porphyrins filtered through the unmodified membrane.

The immobilization of porphyrin nanorods by filtration method resulted in slight alteration of the optical properties. The featureless UV-VIS trace of the $[H_4TPPS_4]^{2-}$ monomer solution filtered through the unmodified membrane indicates that no aggregates formed on the surface of the membrane, Figure 17. This was expected due to the negative charge on the surface of the unmodified membrane. In contrast, the $SnTPyP^{2+}$ solution that was filtered through the unmodified membrane had a peak at 424.5 nm, compared to 417 nm for the free solution.This shift in the Soret and B bands (554 nm, vs. 551 nm and 584 nm) are an indication of ionic self-assembly of the porphyrin structures on the membrane surface [42]. A simple filtration of porphyrin nanorods solution through the membrane also resulted in successful incoporation of nanorods on the surface of the membrane, Figure 16 (b). These results clearly demonstrate how ionic interactions can induce porphyrin self-assembly on a solid surface.

The UV-VIS spectra of the PEI-modified membrane samples exposed to the various solutions is shown in Figure 18. The characteristic absorption peaks for $SnTPyP^{2+}$ (417 and 554 nm) as shown in Figure 18 (c) are not observed. Whereas there is a distinctive change in the absorbance

peaks with the membranes exposed to $H_4TPPS_4^{2-}$ Figure 18 (d). The absence of absorbance peaks from the $SnTPyP^{2+}$ exposed membranes is expected, and confirms the positive charge of the membrane as determined by electro-kinetic measurement. The slight change in the absorption intensity of the $H_4TPPS_4^{2-}$ sample can be attributed to formation of nanorods on the charged membrane surface. A similar result was obtained by Schwab *et al*. on glass and mica substrates [43].

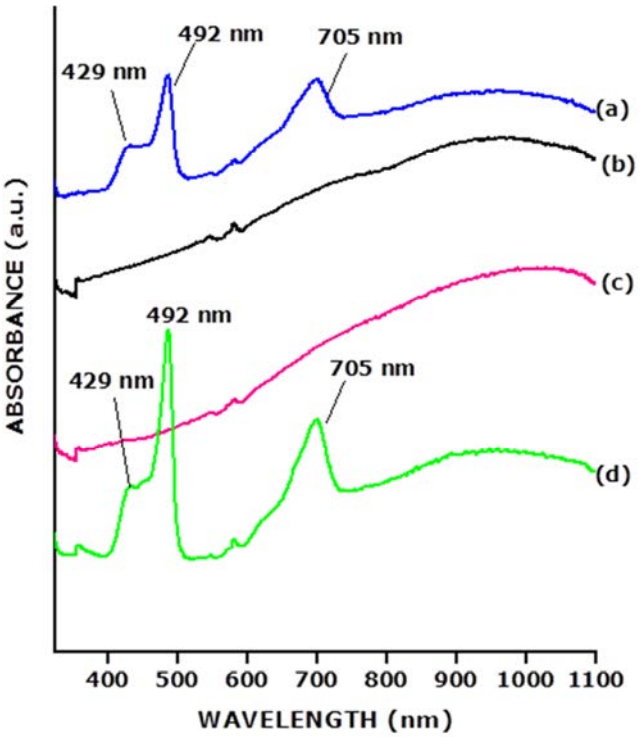

Figure 18. The UV-VIS absorption spectra of (a) modified membrane in the mixture of $H_4TPPS_4^{2-}$ and $SnTPyP^{2+}$, (b) modified membrane before exposure to any solution, (c) modified membrane exposed to $SnTPyP^{2+}$ only, and (d) modified membrane in $H_4TPPS_4^{2-}$ solution.

The formation of nanostructured aggregates, nanorods, by $H_4TPPS_4^{2-}$ on the charged membrane surface can be attributed to the ionic interaction between the negatively charged $H_4TPPS_4^{2-}$ and the positively charged membrane surface. This is in line with literature reports of ionic interactions favouring nanorods and nanotubes formation [42-45]. The peaks observed in this data at 492 nm and 705 nm are characteristic of J-aggregate structures, particularly porphyrin of nanorods [43,45]. The peak at 429 nm is attributed to H-aggregates and the absorbance feature

between 492 and 429 nm is most likely due to a mixture of aggregates and monomer [43]. However, the relatively strong absorbance peak on the modified membrane exposed to $H_4TPPS_4^{2-}$ and then a mixture of $H_4TPPS_4^{2-}$ and $SnTPyP^{2+}$ does suggest the absorbance event is due to various aggregates of $H_4TPPS_4^{2-}$.

4.2.4.3. Self-assembly of porphyrin nanorods on track-etched membranes by a layer-by-layer approach

For the layer-by-layer approach, the PEI-modified membrane was alternatingly immersed in positive and negative porphyrins solutions for about 24 hours. The membrane was dried to get rid of any liquids before the UV-VIS absorption spectra were recorded. This procedure was repeated seven times and the UV-VIS absorption measured after each immersion. Figure 19 shows that after two immersions there are three main absorption bands with peaks at 429, 493, and 706 nm, respectively, and the absorption band between 429 nm and 493 nm is no longer observed. A maximum absorbance was quickly observed after six immersions indicating a complete coverage of the surface of the membrane by the nanorods. At the same time this provides a relatively easy method to track the extent of surface coverage on the membrane. The change in absorbance profile between 429 nm and 493 nm can be attributed to the lack of smaller aggregates or monomer on the PEI-modified membrane due to the longer exposure times.

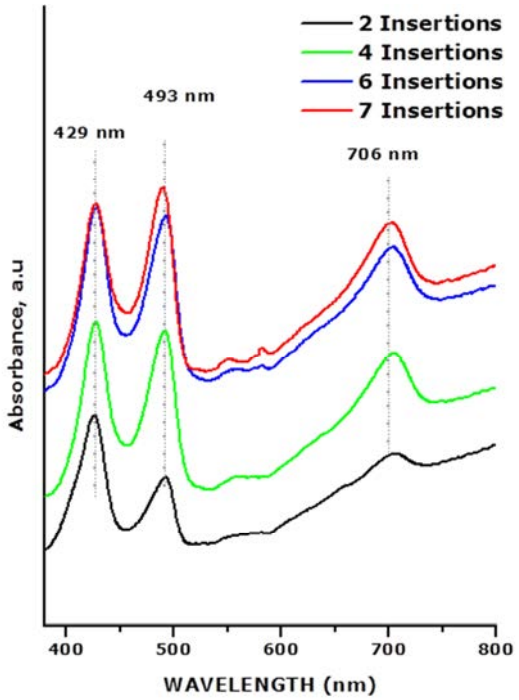

Figure 19. The UV-VIS absorption spectra of modified membrane alternatingly immersed 7 times in $H_4TPPS_4^{2-}$ and $SnTPyP^{2+}$ solutions.

The peaks at 493 nm and 706 nm after immersion are attributed to J-aggregation, and the change in the intensity after each immersions is most likely due to an increase in surface coverage of the J-aggregates, specifically, the porphyrin nanorods. However, the peak at 429 nm undergoes very little change with each immersion, indicating the H-aggregates of $H_4TPPS_4^{2-}$ on the membrane surface have reached the maximum coverage and thus do not change with the subsequent immersions. This could account for an alternative explanation for the change in the intensity of the J-aggregates. The lack of any significant changes with the peak at 429 nm may indicate that the H-aggregates are tethering the nanorods to the membrane surface. The change in peak intensity, at 493 nm and 706 nm, may not be a simple nanorods attachment to the system but more of a re-aggregation of porphyrin structures onto the membrane surface.

SEM observations on the membranes after 2, 4, and 6 immersions are presented in Figure 20. Some of the porphyrin nanorods were aligned vertically and some membrane pores were not blocked by the nanorods. However, by the fourth and sixth immersions as indicated by Figure 20 (b-c), the pores on the PEI modified membrane had lost the characteristic circular shape and adopted a more irregular and slit-like appearance. The use of the layer-by-layer technique

allowed for the vertical alignment and immobilization of the porphyrin nanorods, and when compared to the filtered system, it is expected there will be a greater surface area. The orientation may explain the slightly better absorbance values obtained with the composite system made using the layer-by-layer technique.

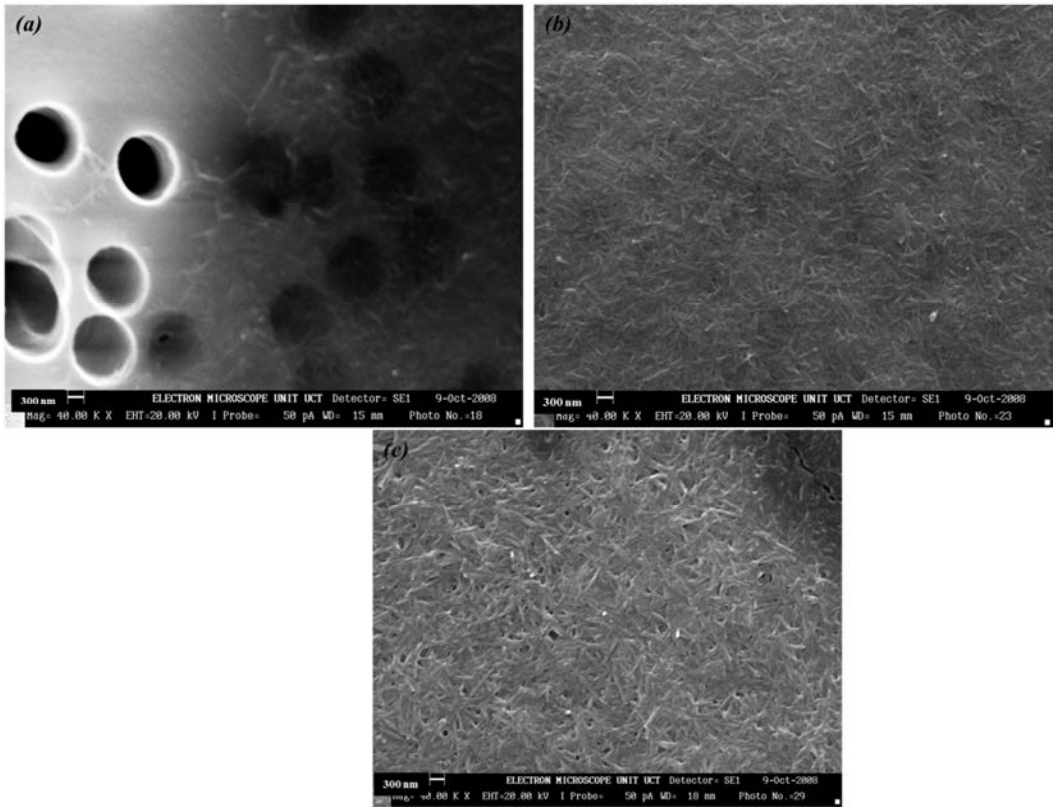

Figure 20.SEM images of the PEI-modified membrane alternatingly immersed in $H_4TPPS_4^{2-}$ and $SnTPyP^{2+}$ solutions, (a) the PEI modified membrane after two insertions, (b) the PEI modified membrane after four insertions and (c) the PEI-modified membrane after six insertions.

4.2.5. Conclusion

PEI was successfully used to modify the overall surface charge of PET track-etched membranes from a net negative to a positive charge at a pH = 6.0. The PEI-modified membrane was then used as a template for the ionic self-assembly of porphyrin nanotubes via a layer-by-layer technique. The characteristic absorption peaks at 423, 493, and 706 nm are indicative of porphyrin nanotubes and were observed using UV-VIS spectroscopy. Unmodified and modified

membranes were able to induce self-aggregation of the porphyrin molecules with the corresponding charges. The use of the unmodified membrane resulted in nanostructure formation with $SnTPyP^{2+}$, whilst the modified membrane induced similar aggregation with the $H_4TPPS_4^{2-}$. The nanorods formed an interwoven network on the surface of the membranes even with pore diameters greater than the average length of the nanorods (400 – 600 nm). UV-VIS comparison of the filtration and the layer-by- layer technique resulted in slightly different absorbance values. The layer-by-layer technique gave different absorption values which could be attributed to the difference in orientation of the nanorods on the surface of the membrane. The assembly of porphyrin nanotubes on track-etched membranes can be easily achieved through altering the surface charge of the respective membranes.

4.3. Porphyrin nanorods-polystyrene composite by latex blending

4.3.1. Introduction

Latex blending is a preferred method as it is easy to produce and enables nano-fillers to be incorporated into any type of highly viscous polymer such as polystyrene. As mentioned in Chapter 2, most nanocomposites exploit CNTs as conductive filler dispersed into an insulating matrix. We attempted to produce similar composites using porphyrin-based nanorods as filler. As has been reported for CNTs, porphyrin nanorods produced in this current study are also tightly bundled and as a result this limits their use as filler in a polymer matrix. The challenge is therefore to incorporate individual nanorods, or at least relatively thin nanorods bundles, inside a polymer matrix in order to obtain dispersion. The resulting composites consisted of dispersed nanorods in a polymer matrix. In this study optical, dispersion and morphological properties of the porphyrin nanorods-polystyrene composite were investigated. The porphyrin nanorods were prepared by ionic self-assembly and polystyrene latex by free radical emulsion polymerization.

4.3.2. Materials and Methods

Table 3. Table showing components of free-radical emulsion polymerization of styrene.

Component	Mass (g)
Styrene	63
Water	178.05
Triton X100	6.5
Sodiumcarbonate	0.175
Sodium peroxydisulfate	0.1125
Dodecyl mercaptan	0.002

The reaction was performed in a 250 mL glass reactor with an impeller speed of 400 rpm at 70 °C. The reactor was charged with styrene, Triton X100, sodium carbonate (Na_2CO_3) and water. Prior to the reaction, styrene was passed through an inhibitor-remover column to remove 4-tert-butylcatechol (TBC), which influences the course and outcome of the emulsion polymerization process [46]. The reaction mixture was degassed to remove the oxygen, by purging with argon, for 15 minutes. A solution of sodium peroxydisulfate ($Na_2S_2O_8$) in water was also degassed. In the other reaction, a chain transfer agent (CTA) was added to the reaction mixture in order to control the molecular weight of the latex. The reaction was started upon the introduction of the initiator solution, and the reaction time was about 5 hours. The latexes were dialyzed for 4-6 days against double deionized water to remove excess surfactant and the water was replaced every 24 hours. Dialysis was done because a large excess of surfactant was used in the emulsion preparation. Snake-skin pleated dialysis tubing of 3500 MW cut-off was used.

For composites preparation, the final polystyrene latex was mixed with different quantities of porphyrin nanorods and the mixtures were then rapidly frozen using liquid nitrogen and freeze dried overnight with a Christ Alpha 2-4 freeze dryer. Lastly, the freeze-dried product obtained was compression moulded into 1 ~ 2 mm thick disk type samples with diameter of 25 mm at 180 °C and 100 bar for 2-3 minutes using a hot press on a temperature controlled Graseby Specace Press.

4.3.3. Characterization techniques

The particle morphology of the latex particles were investigated by Zeiss 912-Omega TEM. To prepare samples for TEM analysis, about 1µL of the polystyrene latex was diluted with~1 mL of double deionised water so as to obtain a translucent solution. The sample solution was dropped on to a carbon-coated 200 mesh copper grid and left to dry at room temperature before the imaging was done. The molecular weight and its distribution of the latex were determined using size exclusion chromatography (SEC).The SEC instrumental set up comprised of a Shimadzu LC-10AT isocratic pump, a Waters 717 plus auto-sampler, a refractive index detector, a Waters 2487 dual wavelength UV detector, Waters Alliance apparatus fitted with a 50 × 8 mm guard column connected in series with three 300 × 8 mm, 10 µm particle size, GRAM columns (2 × 3000 Å and 100 Å). The columns were calibrated with polystyrene standards and the mobile phase was THF (stabilized by 0.125% BHT) with a flow rate of 1.00 mL/min. Particle size distribution was determined using Malvern Zeta Sizer Nano-S instrument. The particle size was measured at a 90 degree scattering angle using DLS. He-Ne laser of wavelength 633.0 nm was used and the instrument was calibrated with 200 nm polystyrene spherical particles. The samples were diluted until slightly transparent and the average of 3 measurements of 14 acquisitions on each sample was conducted. The morphology of freeze-dried polystyrene-porphyrin nanorods films were characterized using a Leica-LEO Stereoscan S440 and FEI Nova NanoSEM 50 series electron microscopes. Porphyrin nanorods-polystyrene films were also analysed CECIL 2021 UV-VIS spectrophotometer. FT-IR spectra were measured to identify the functional groups on porphyrin nanorods-polystyrene using a Perkin Elmer spectrum 1000 FT-IR spectrometer. The range of 400–4000 cm^{-1} was examined to detect the presence of specific functional groups in the samples. Inverted Olympus IX-81 fluorescent microscope with an F-view-II cooled CCD camera was used to investigate the dispersion state of porphyrin nanorods in polystyrene matrix. The polystyrene-porphyrin nanorods films were excited by exposure to 561 nm using a Xenon-Arc burner (Olympus Biosystems GMBH). For the z-stack image frame acquisition, an Olympus UPlan Apo N 100× oil objective and the cell^R imaging software were used.

4.3.4. Results and discussion

4.3.4.1. Polystyrene latex characterization

The particle morphology of the latex was investigated by means of TEM and the micrographs were obtained. The micrographs show spherical polydispersed particles. For Figure 21 *(a),* DLS results showed that average diameter of latex was 196.3 nm with a distribution index of 0.05 and -51.6 mV zeta (ζ) potential. The SEC data showed a number average molecular weight (M_n) of 678 306 and weight average molecular weight (M_w) 934 646 with dispersity (*Đ*) of 1.37. For Figure 21 *(b),* DLS results showed that the latex had average diameter of 125.6 nm with distribution index of 0.013 and ζ-potential was -37.1 mV. The M_n for this latex was 91 582 and M_w of 669 553 with *Đ* of 7.2.

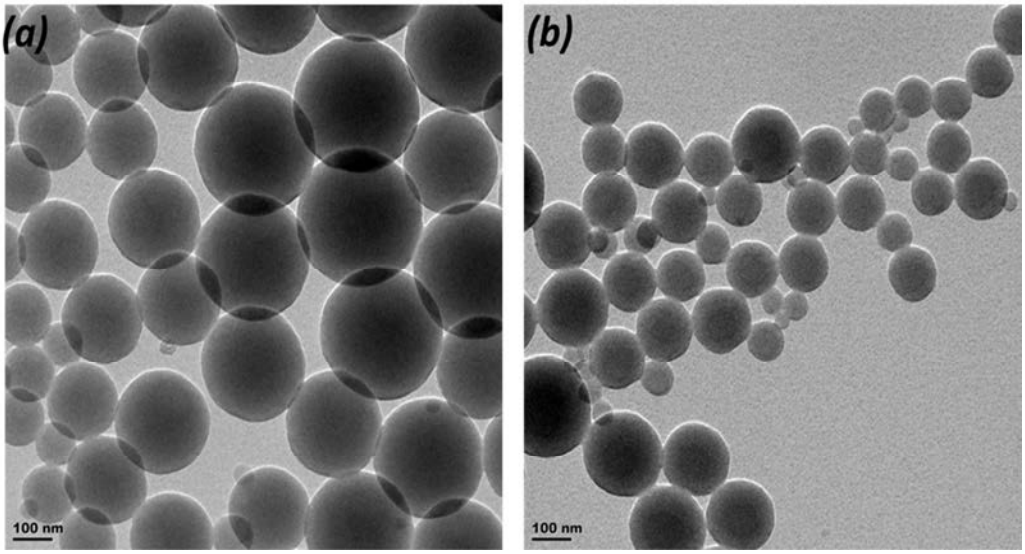

Figure 21. TEM micrographs of the final polystyrene latex of emulsion polymerization with Triton X 100 surfactant, (a) no CTA used, (b) dodecyl mercaptan used as a CTA.

Investigations on the structure of freeze-dried compression-moulded composite films were performed using SEM. The SEM images of the surface of the porphyrin nanorods-polystyrene composite films, Figure 22, show two distinct regions; one containing white spots; representing the nanorods and the other free of white spots. The secondary electron yield is enriched at the location of the nanorods, which results in the contrast between the nanorods network and the polymer matrix.

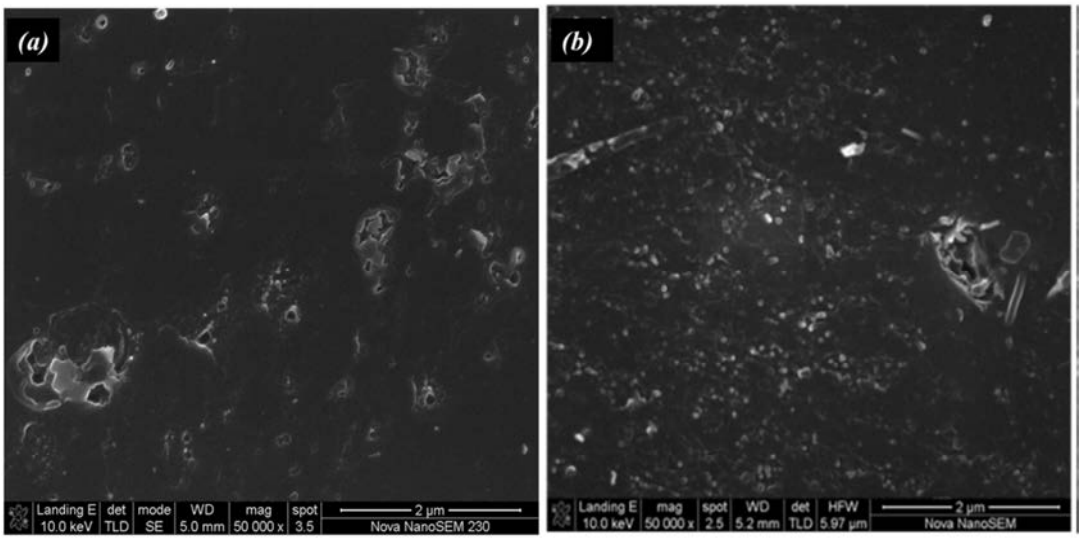

Figure 22. SEM image of the surface of a (a) 0.5 wt %, (b) 1 wt % porphyrin nanorods-polystyrene without CTA composite.

The SEM investigation in this study provided information on the distribution state of nanorods in the polystyrene matrix. In the case of higher nanorods loadings (7 – 10 wt %) a larger number of cylindrical-like structures were observed. As observed in Figure 23, it can be deduced that the white spots observed are the porphyrin nanorods in the polymer matrix.

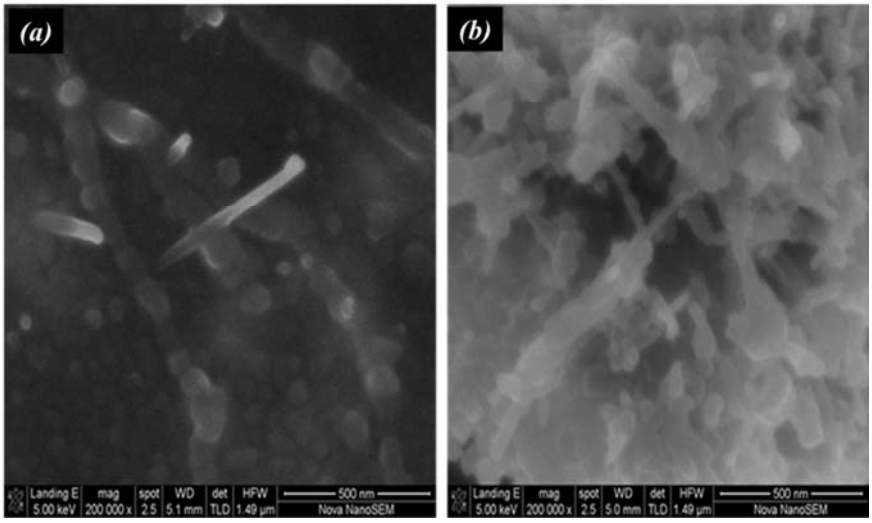

Figure 23. SEM images of the surface and internal structure of porphyrin nanorods-polystyrene composite. (a) 7 wt %, (b) 10 wt % porphyrin nanorods in polystyrene without CTA.

4.3.4.2. Porphyrin nanorods-polystyrene composites FT-IR characterization

Freeze-dried and compression moulded films were investigated by means of FTIR transmission spectroscopy. FTIR measurements were conducted particularly to provide information on the bonds involved in the interaction of polystyrene with porphyrin nanorods.

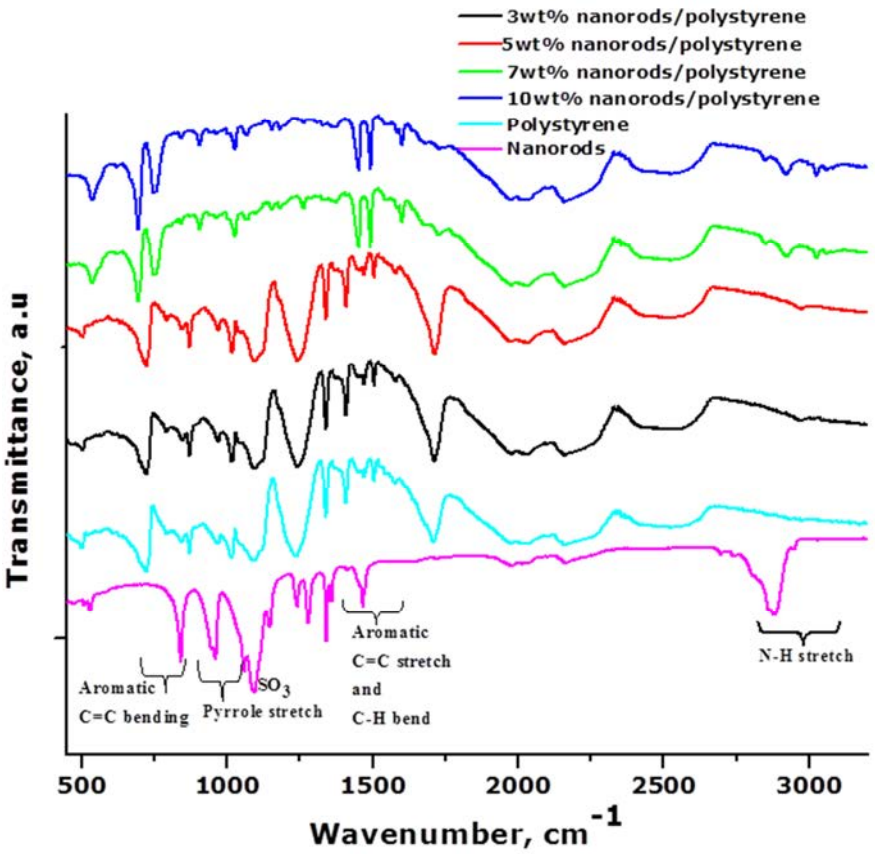

Figure 24. The IR spectra of porphyrin nanorods-polystyrene composites of different wt %.

In Figure 24, the spectra for the porphyrin nanorods, most of the bands that appear in the low wave number region (456 — 979 cm^{-1}) are due to the in-plane bending, out-of-plane bending, ring rotation, and ring torsion modes of porphyrin skeletal. In the case of polystyrene in the low wave number region the bands appear at ~750 cm^{-1} due to C - H bond and as the wt % of porphyrin nanorods in polystyrene increases there are new peaks that appear at ~900 cm^{-1} and 904 cm-1 for 7 wt % and 10 wt % respectively. The new vibration modes assigned to the aromatic ring at ~900 cm^{-1} and 904 cm^{-1}. It was also observed that as the wt % increases both the nanorods bands and broad polystyrene bands that appear in the region ~ 1237 cm^{-1} and 1240 cm^{-1}

disappear. This is due to the vibrational stretching of the benzene ring in both the polystyrene and porphyrin molecules as they start interacting. For the 10 wt % sample the vibration peaks of the aromatic ring appear at 1446 cm^{-1}, 1501 cm^{-1} and 3024 cm^{-1} are due to C = C stretching and C - H respectively. The shift of the C = C stretching peak is due to π-π interaction between the phenyl ring of the polystyrene and the porphyrin nanorods wall. The peaks of the aromatic ring of the 7 wt % sample appear at 1419 cm^{-1}, 1493 $cm^{-1}$and 2996 cm^{-1}. For the 5 wt % sample the peaks of the aromatic ring appeared at 1439 cm^{-1}, 1602 $cm^{-1}$and 3031 cm^{-1} and for the 3 wt % sample the peaks appeared at 1413 cm^{-1} and 1473 cm^{-1}. The N - H stretching vibrations are observed at 3325 cm^{-1} for the 5 wt % and 10 wt % samples, and at 3302 cm^{-1} for the 7 wt % sample. This corresponds to the stretching vibration in the porphyrin molecules which further indicate the presence of porphyrins in the composite sample. The N - H stretching bands were more pronounced in the cases of the 7 wt % and 10 wt % samples where the wt % of the porphyrin nanorods in the polystyrene was higher. As the wt % of the nanorods in the polystyrene increases the spectral pattern followed coincided with that of the porphyrin nanorods.

4.3.4.3. Porphyrin nanorods-polystyrene composites fluorescence microscopy characterization

Freeze-dried and compression moulded porphyrin nanorods-polystyrene films were viewed via fluorescence microscopy to determine the distribution of porphyrin nanorods within the polymer matrix. The fluorescence images, Figure 25 were acquired for composites containing 1, 5, 7 and 10 wt % of porphyrin nanorods in polystyrene. Fluorescence was also detected from agglomerated nanorods as they exhibited intense fluorescent signals. The fluorescing aggregates appeared to be distributed evenly throughout the film for the 7 and 10 wt % samples. Due to lower amount of porphyrin nanorods present for 1 and 5 wt % film samples in Figure 25 (a) and (b), the fluorescing aggregates were only observed in some part of the film.

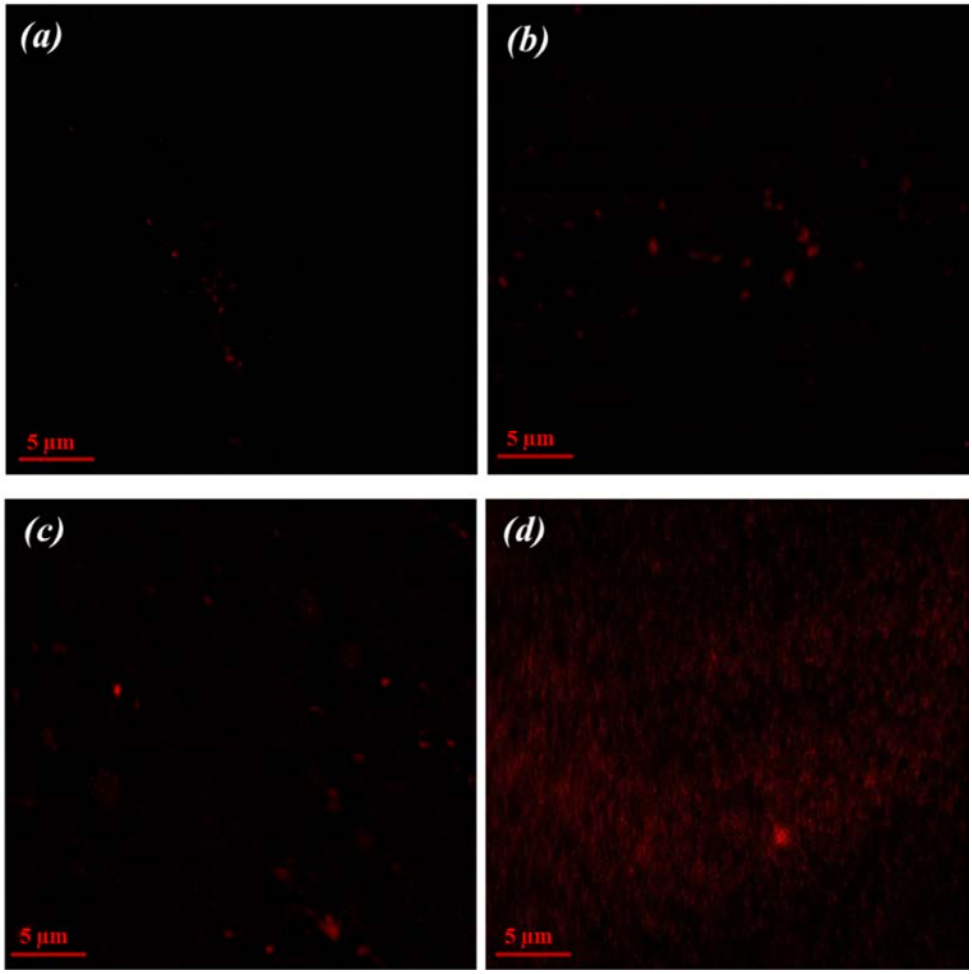

Figure 25. Fluorescence microscopy images of porphyrin nanorods-polystyrene composites containing (a) 1 wt %, (b) 5 wt %, (c) 7 wt % and 10 wt % porphyrin nanorods.

In terms of energy transfer, in a natural light harvesting system once the pigment is excited it will either transfer energy to another pigment or emit this energy as a photon (fluorescence). Energy transfer to another molecule is usually faster and if the molecules are far apart or damaged this process will be slower or will not happen in which case they will fluoresce [47]. The fluorescence images did not display much fluorescence within the composite and it was therefore assumed that the porphyrin nanorods were connected and well blended within the polymer matrix. We at this point cannot make any conclusions regarding the dispersion of nanorods within the matrix.

4.3.4.4. Porphyrin nanorods-polystyrene composites UV-VIS absorption characterization

The incorporation of porphyrin nanorods in a polymer matrix by latex blending method exhibited peaks both in the UV-VIS and near IR regions. The absorbance spectra of porphyrin nanorods – polystyrene exhibited characteristics related to porphyrin nanorods in solution.The sharp absorption peaks observed at 450 nm are indicative of the presence of well-defined stacks of porphyrin molecules [48]. These peaks are an indication of successful incorporation of the nanorods in polystyrene matrix. As expected intense absorbance band was observed for the 10 wt % sample due to a large number of nanorods present in the polystyrene.

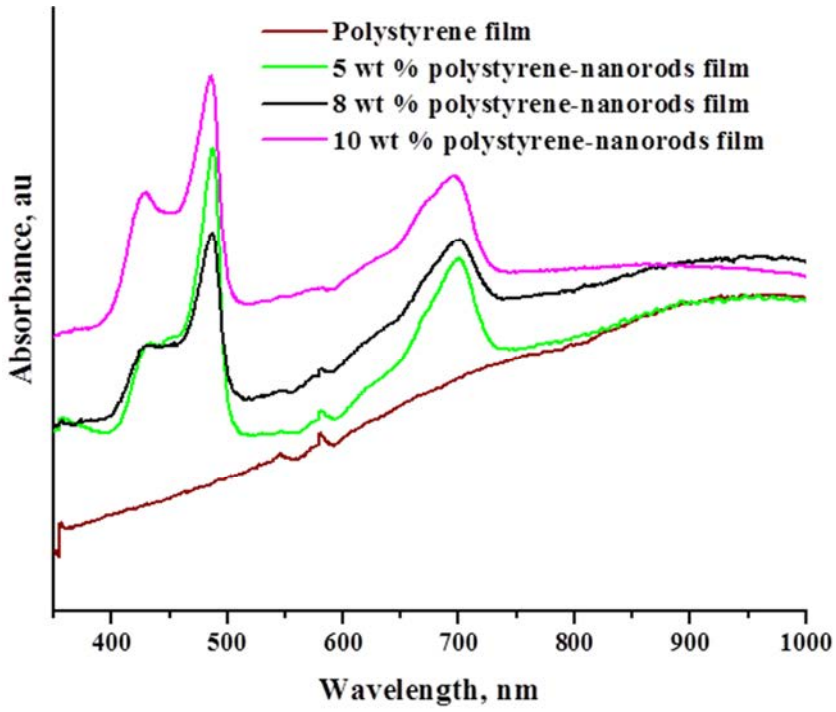

Figure 26. The UV-VIS absorption spectra of porphyrin nanorods-polystyrene composites of different wt %.

The incorporation of porphyrin nanorods into polymer matrices can be challenging since the optical properties can significantly change upon altering the environment. Using latex blending and self-assembly on the membrane surface allowed for the transfer of nanorods from solution

onto surface while maintaining the UV-VIS and near IR absorption properties of the porphyrins in solution.

4.4. Porphyrin nanorods-polymer composite by electrospinning

4.4.1. Introduction

In terms of the principles of electrospinning it is expected that the nanorods would align during the process as this was also previously predicted mathematically [15]. The quality of nanoparticles dispersion in the polymer solution has a significant influence on the distribution and alignment of the nanoparticles in the fibres. The final fibre structure and diameter is dependent on a number of parameters as discussed in Chapter 2. We attempted to incorporate porphyrin nanorods into fibres by electrospinning. The morphological properties of PEO and polystyrene fibres were studied to determine the effect of porphyrin nanorods.

4.4.2. Materials and Methods

Sample preparation

PEO fibres: 4 and 8 wt% PEO and PEO-porphyrin nanorods solutions (PEO, Sigma Aldrich, M_w = 300,000) were prepared using deionized water followed by continuous 24 hours of stirring. The solution was loaded into a horizontally held pasteur pipette. The pipette is fitted over a positive electrode lead connected to a voltage power supply that can generate direct current (DC) voltages up to 25 kV. In order to charge the PEO-porphyrin nanorods solution a copper wire was inserted into the pasteur pipette to act as the electrode. A grounded board covered with aluminium foil was placed ~ 27 cm away from the pipette tip. Silicon substrates were fixed on the aluminium foil to collect the electrospun fibres for characterization. Electrospinning was carried out in air at applied voltages that ranged from 10 kV to 20 kV and the spinning time was ~30 minutes.

Polystyrene fibres: 10 wt % of spinning solutions were prepared by dissolving freeze-dried polystyrene latex and polystyrene latex-porphyrin nanorods samples (M_n = 678 306) in

tetrahydrofuran (THF). The polymer was dissolved at room temperature with 8 hours of stirring. The electrospinning apparatus consisted of a 1 mL syringe connected to a syringe pump to supply a steady flow of 0.09 mL/min of solution to the tip of the needle. A high-voltage power supply was used to apply a potential of 20 kV to the syringe needle. An aluminium foil covering the rotating drum was placed ~20 cm from the needle tip to collect the fibres.

4.4.3. Characterization techniques

The electrospun fibres were characterized using SEM and TEM. The infrared spectra of fibres deposited on aluminium foil were recorded in transmission mode. SEM and TEM experimental set-up have been discussed in detail in Section 3.1.4 and FT-IR in Section 4.2.3.

4.4.4. Results and discussions

4.4.4.1. PEO fibres characterization

SEM analysis was used to investigate the morphology of PEO fibres as well as PEO fibres with porphyrin nanorods. The electric field strength is known to increase with increasing voltage and that enhances the electrostatic force on the solution jet which in turn favours formation of thinner fibre [49]. The applied voltage was varied from 10- 20 kV during electrospinning of PEO. The fibres diameters were observed to decrease with increase in applied electrical voltage. Another observation was the formation of beaded fibres which also depended on the applied voltage, Figure 27 (a-c). An increase in the applied voltage reportedly favours the formation of fibres with high bead density. The amount of beads was significantly less for 10 kV as compared to 25 kV. The spinning voltage is strongly linked with the formation of bead defects in the fibres [50]. At lower voltage the flight time of the fibre to the collector increases leading to formation of fine fibres. There is greater tendency to bead formation at high voltage because of increased instability of the Taylor cone.

The average fibre diameters of collected fibres are given in Table 4.

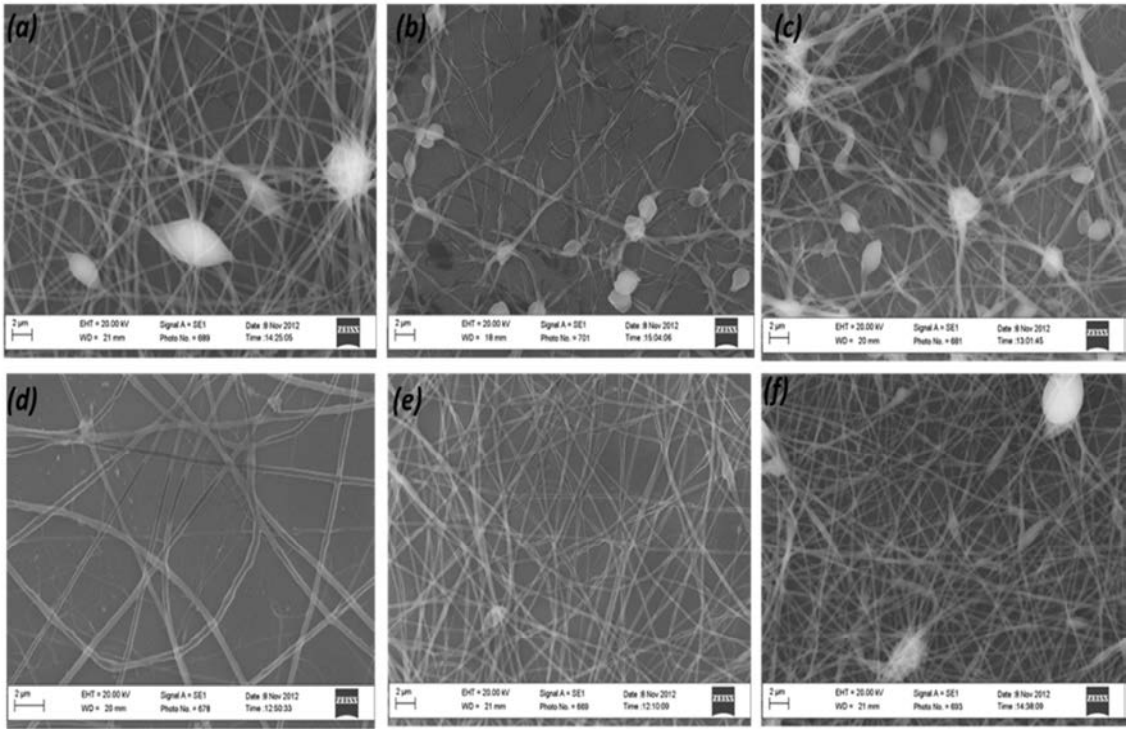

Figure 27. SEM micrographs of electrospun PEO fibres from (a-c) 4 wt % at voltages 10, 15 and 20 kV respectively and (d-f) 8 wt % at 10, 15 and 20 kV respectively.

The presence of porphyrin nanorods in the fibres was confirmed also by SEM and TEM analysis. The fibres appear to be swollen with humps and other fibres were broken. An increase in fibres diameters was also observed due to the presence of nanorods inside the fibres. The SEM images also revealed nanorods protruding from the ends of broken PEO fibres, Figure 28. The diameter of protruding nanorods measured from SEM images ranged from 30 to 63 nm. This was not surprising since the average diameters of the nanorods before electrospinning solution preparation was between 20 nm and 60 nm, and this slight increase may have been due to small layer of polymer covering the rods.

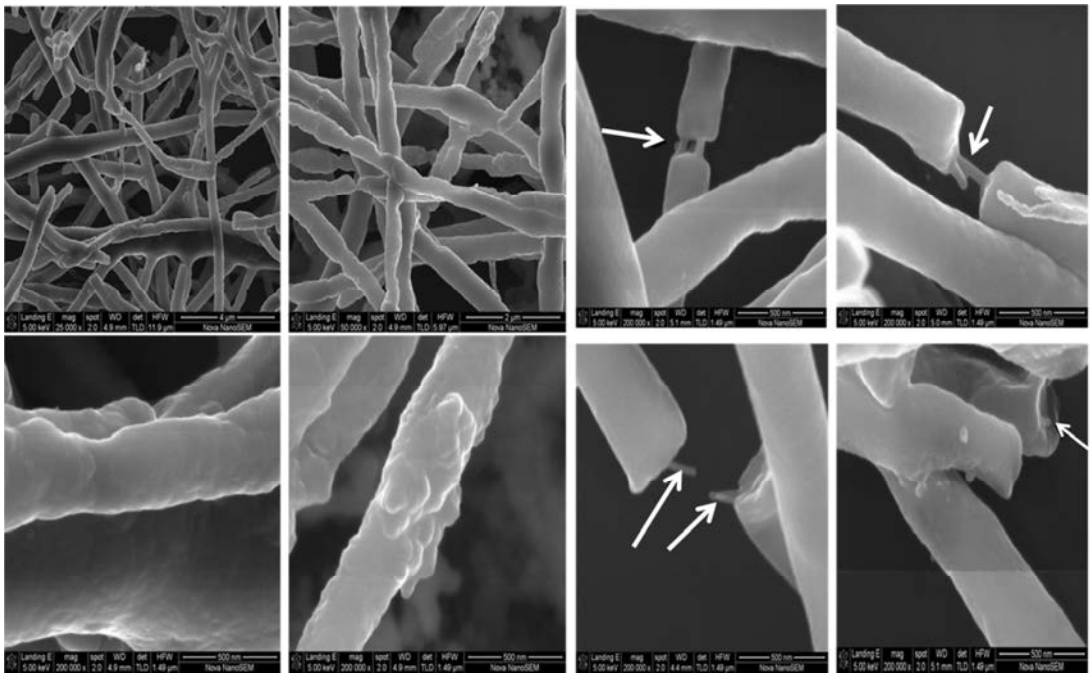

Figure 28. SEM images of PEO electrospun fibres with porphyrin nanorods.

Table 4. The average diametres (nm) of PEO and PEO-porphyrin nanorods fibres. (Sample A: 10.5 µM $H_4TPPS_4^{2-}$, 0.02 M HCl : 3.5 µM $SnTPyP^{2+}$) (sample B: 21 µM $H_4TPPS_4^{2-}$, 0.02 M HCl : 7µM $SnTPyP^{2+}$)

Voltage Applied	PEO	Sample A	Sample B
10 kV	518	404	295
15 kV	400	391	290
20 kV	333	235	285

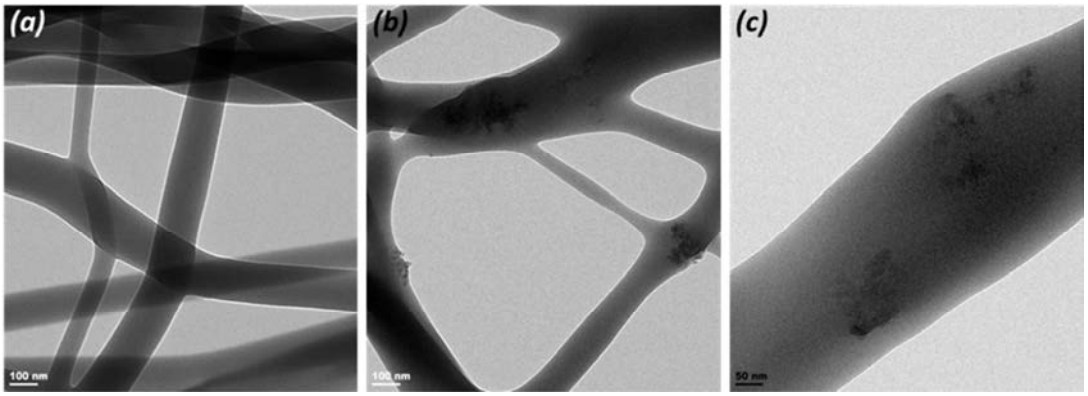

Figure 29. TEM images of (a) pure PEO fibre (b-c) PEO fibres with nanorods. PEO solution concentration= 8wt%.

The fibres electrospun from porphyrin nanorods-PEO solution were viewed under TEM, Figure 29, and some dark areas were observed in the fibres. The dark areas in the fibres are thought to be porphyrin nanorods agglomerates within the PEO matrix. Although the nanorods are prone to agglomeration, formation of agglomerates may also have resulted from the mixing process during solution preparation or from settling of the particles from the polymer solution. PEO-porphyrin nanorods fibres consisted of aggregated porphyrin nanorods inside the fibres and randomly distributed along the length of fibres. The electrospinning process can handle dispersions of poor quality and this may affect the alignment and distribution of nanotubes embedded in the fibres [14].

4.4.4.2. PEO-porphyrin nanorods FT-IR characterization

In order to determine the interactions between PEO and porphyrin nanorods fibers, FTIR spectra were acquired. The spectra in Figure 30 showed that the bands for vibrations of $–CH_2–$ group appeared at about 1284 and 1467 cm^{-1} and for the asymmetric stretching vibration of the C–O group the bands were observed at about 1093 and 962 cm^{-1}. Broad bands near 2890 cm^{-1} are assigned to the aliphatic C–H stretching mode of the PEO units. The spectra also showed stretching vibration bands at 1589 and 1475 cm^{-1} attributed to C=C and ring bending vibration bands around 1000 cm^{-1} region attributed to C-H of the phenyl groups of porphyrin molecules. A broad band at 2944 cm^{-1} which is related to N - H and C-H stretching vibrations of the porphyrin was observed. Comparing the spectra in Figure 30, one could observe that the band at 2944 cm^{-1}

which is related to N - H was also present in the porphyrin nanorods - PEO fibres. The intensities and widths of the bands at 1284 and 1467 cm^{-1} were decreased. These observations suggested that there were some chemical interactions between PEO and porphyrin molecules. The fibres were electrospun at different voltages and no significant difference was observed.

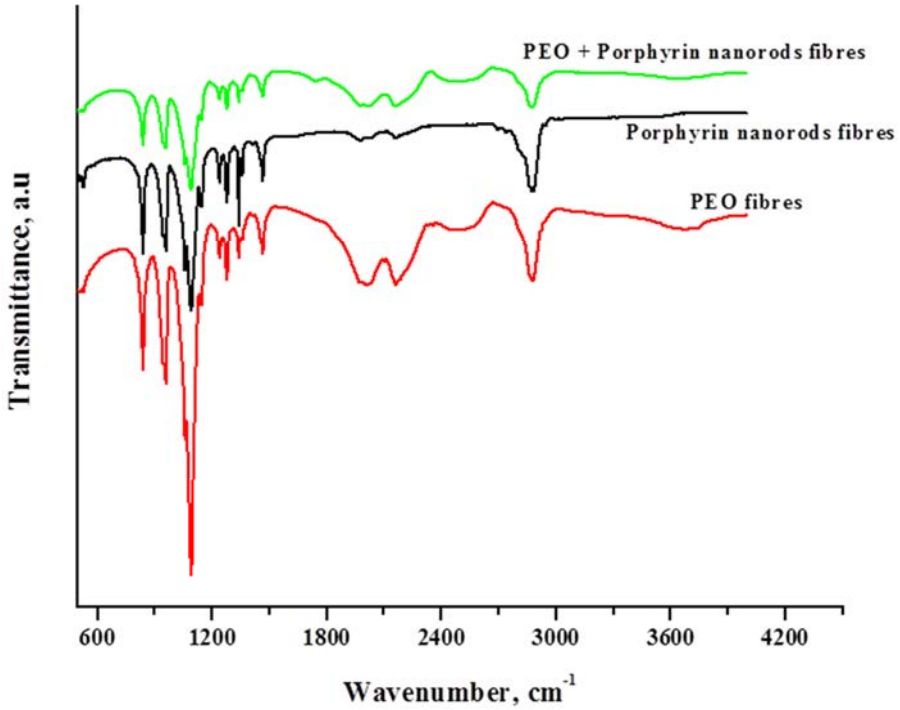

Figure 30. The IR spectra of electrospun PEO, porphyrin nanorods, and PEO+ porphyrin nanorods fibres.

4.4.4.3. Polystyrene fibres characterization

SEM analysis was used to investigate the morphology of polystyrene fibres and the average diameters for both fibres with and without porphyrin nanorods were determined. The fibres average diameter for fibres without nanorods ranged from 1 - 7 µm and those with nanorods ranged from 2 – 11 µm. The fibres appeared to have rough continuous stripes-like morphology along the axial direction on the fibre surface. The wrinkled fibre structure observed may be due to the fast evaporation of THF. The images also showed that polystyrene fibres with porphyrin nanorods were rough with stripe-like morphology, Figure 31 (d). The problem encountered during the electrospinning process of the polystyrene in THF, was the congestion of solution at the tip of the syringe due to the fast evaporation of THF which has a low boiling point [6].

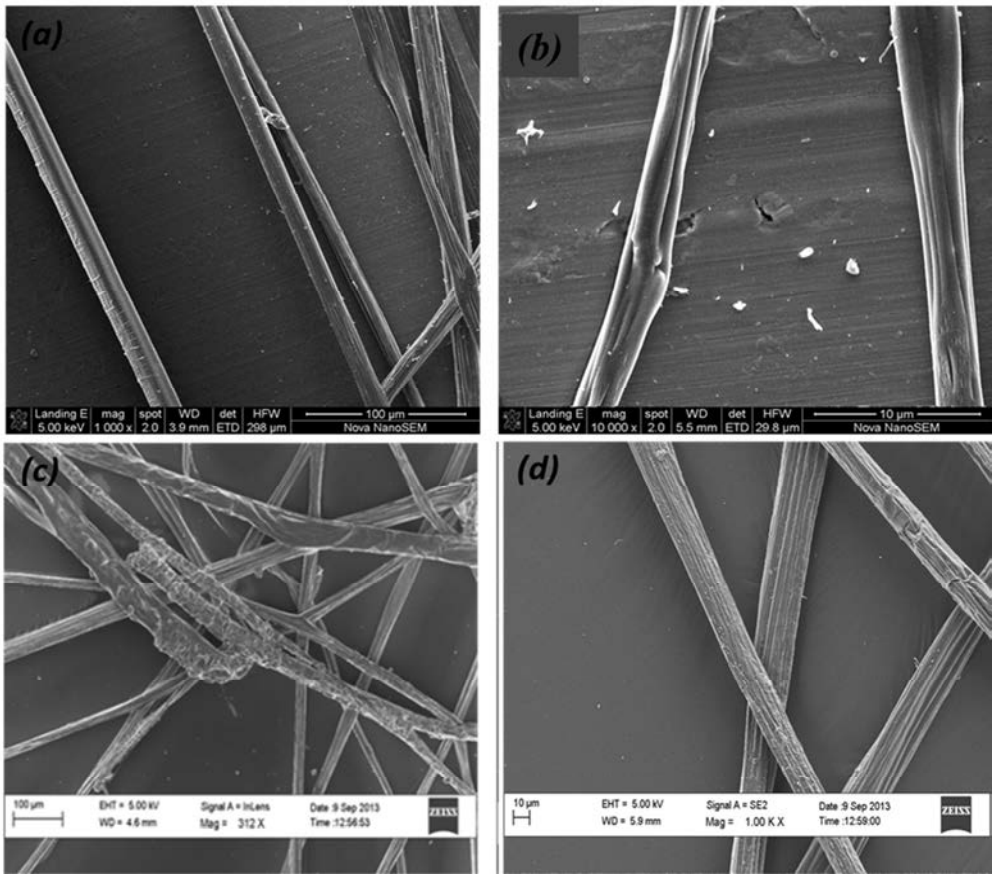

Figure 31. SEM micrographs of polystyrene fibres (M_n = 678 306) (a-b) without porphyrin nanorods and (c-d) with 10 wt % porphyrin nanorods.

The fibres appeared to have surface roughness as depicted in Figure 32. Parameters such as humidity and temperature were not controlled and it was not easy to compare or explain this roughness.

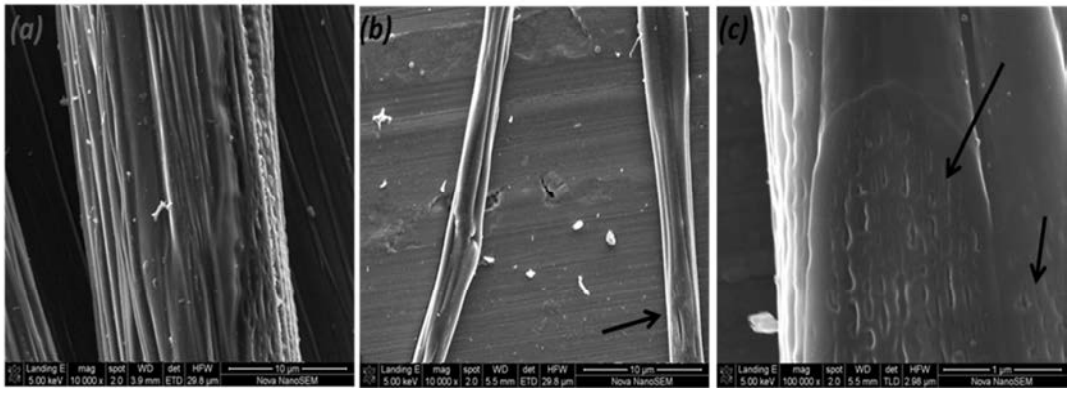

Figure 32. SEM micrographs showing polystyrene fibres with roughness on the surfaces.

4.4.4.4. Porphyrin nanorods-polystyrene electrospun fibres fluorescence microscopy characterization

The advantage of using fluorescence microscopy is the ability to obtain information on the distribution of nanorods in fibres. Figure 33 shows fluorescence micrographs of electrospun polystyrene fibres with porphyrin nanorods. The fibres showed fluorescent behavior and this were observed along the lengths of the fibres. Some fibres showed little fluorescence but as expected fibres with 5 wt % porphyrin nanorods fluoresce less than the fibres with 10 wt % nanorods. The observation of fluorescence from porphyrin nanorods is expected to be of considerable importance in photonics applications.

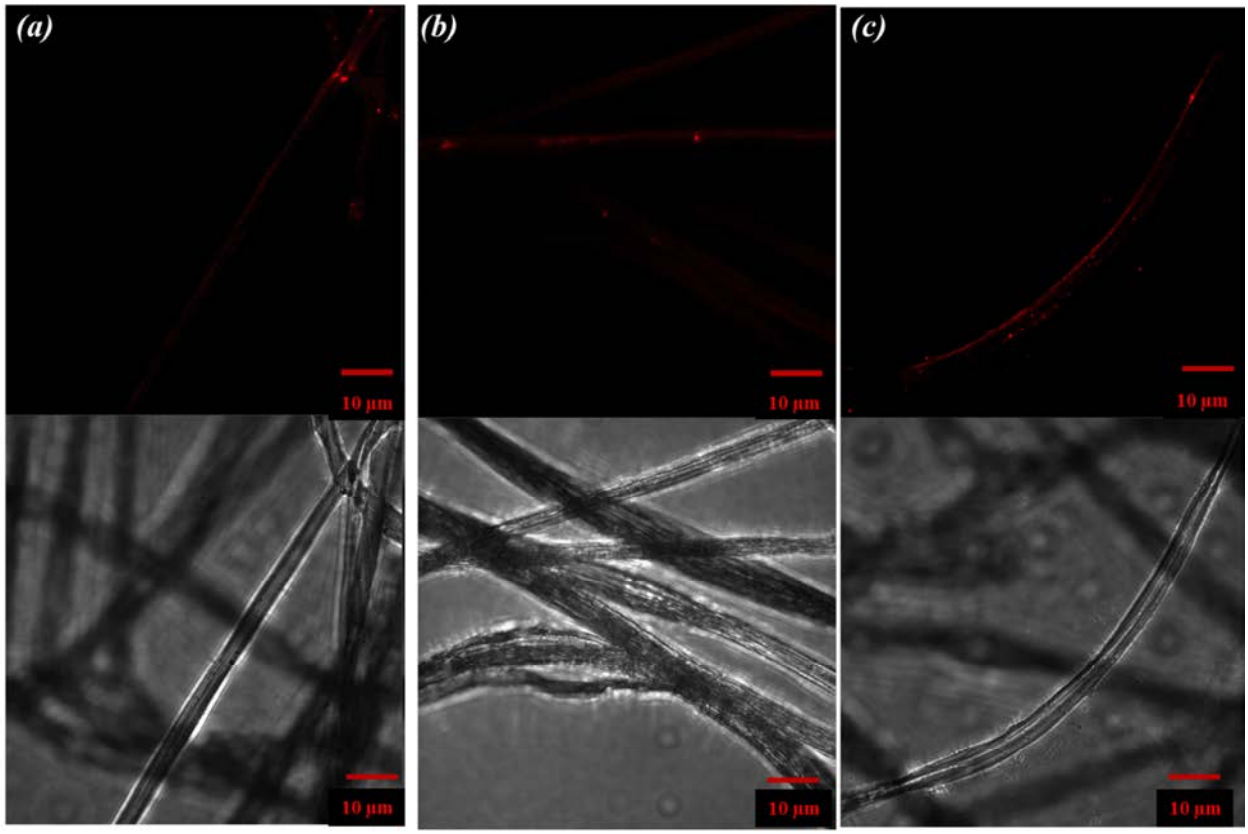

Figure 33. Fluorescence microscopy images of porphyrin nanorods-polystyrene electrospun fibres containing (a) 5 wt %, 8 wt % and 10 wt % porphyrin nanorods.

4.5. Conclusion

The incorporation of nanorods in polymer matrices by latex blending, electrospinning and by self-assembly on track-etched membrane was achieved. The incorporation into matrices addressed the issue of handling the porphyrin nanorods in solution and fulfilled the requirement of use of appropriate support for their use as devices. The composites produced by latex blending resulted in porphyrin nanorods distribution throughout the film surface. The latex blending approach allows one to control the properties of nanorods, the ability of which is expected to be useful for the fabrication of optical devices. We also fabricated fluorescing polystyrene-porphyrin nanorods fibres using the electrospinning technique. Adding porphyrin nanorods to the polystyrene had an effect on the morphology of the fibres with a slight increase in the fibres diameters. The PEO fibres showed nanorods protruding from the ends of broken fibres and this was observed without any difficulty. The self-assembly of porphyrin nanorods on the surface track-etched membrane using a layer-by-layer technique showed desired absorbance signature (UV-VIS and near IR region) for solar radiation harvesting applications and this observations make them potentially useful for application as antennae in artificial light harvesting systems.

4.6. References

[1] G. McDermott, M. Prince, A. Freer, M. Hawthornthwaite-Lawless, Z. Papiz, R. Cogdell, and W. Isaacs, *Nature,* **374**, 517-521 (1995).

[2] X. Hu, A. Damjanović, T. Ritz, and K. Schulten,*Proc. Natl. Acad. Sci.,* **95**, 5935-5941 (1998).

[3] L. Valkunas, E. Akesson, T. Pullerits, and V. Sundström, *Biophys. J.,* **70**, 2373-2379 (1996).

[4] C.J. Murphy and C.J. Orendorff, *Adv Mater,* **17**, 2173-2177 (2005).

[5] M. Sykora, K.A. Maxwell, J.M. DeSimone, and T.J. Meyer, *Proc. Natl. Acad. Sci.,* **97**, 7687-7691 (2000).

[6] D.A. Higgins, J. Kerimo, D.A.V. Bout, and P.F. Barbara, *J. Am. Chem. Soc.,* **118**, 4049-4058 (1996).

[7] V. Balzani, A. Juris, H. Venturi, S. Campagna, S. Serroni, and G. Denti, *Solar Energy Mater. Solar Cells,* **38**, 159-173 (1995).

[8] O. Regev, P.N.B. ElKati, J. Loos, and C.E. Koning, *Adv Mater,* **16**, 248-251 (2004).

[9] J. Loos, A. Alexeev, N. Grossiord, C.E. Koning, and O. Regev, *Ultramicroscopy,* **104**, 160-167 (2005).

[10] X. Xu, M.M. Thwe, C. Shearwood, and K. Liao, *Appl. Phys. Lett.,* **81**, 2833-2835 (2002).

[11] R. Haggenmueller, H. Gommans, A. Rinzler, J.E. Fischer, and K. Winey, *Chem. Phys. Lett.,* **330**, 219-225 (2000).

[12] M. Manchado, L. Valentini, J. Biagiotti, and J. Kenny, *Carbon,* **43**, 1499-1505 (2005).

[13] P. Pötschke, A.R. Bhattacharyya, and A. Janke, *Carbon,* **42**, 965-969 (2004).

[14] W. Salalha, Y. Dror, R.L. Khalfin, Y. Cohen, A.L. Yarin, and E. Zussman, *Langmuir,* **20**, 9852-9855 (2004).

[15] Y. Dror, W. Salalha, R.L. Khalfin, Y. Cohen, A.L. Yarin, and E. Zussman, *Langmuir,* **19**, 7012-7020 (2003).

[16] F. Ko, Y. Gogotsi, A. Ali, N. Naguib, H. Ye, G. Yang, C. Li, and P. Willis, *Adv Mater,* **15**, 1161-1165 (2003).

[17] L.Y. Yeo and J.R. Friend, *J. Exp. Nanosci.,* **1**, 177-209 (2006).

[18] Z. Zhou, C. Lai, L. Zhang, Y. Qian, H. Hou, D.H. Reneker, and H. Fong, *Polymer,* **50**, 2999-3006 (2009).

[19] S.D. McCullen, D.R. Stevens, W.A. Roberts, S.S. Ojha, L.I. Clarke, and R.E. Gorga, *Macromolecules,* **40**, 997-1003 (2007).

[20] B. Sundaray, V. Subramanian, T. Natarajan, R.Z. Xiang, C.C. Chang, and W.S. Fann, *Appl. Phys. Lett.,* **84**, 1222-1224 (2004).

[21] F. Ko, Y. Gogotsi, A. Ali, N. Naguib, H. Ye, G. Yang, C. Li, and P. Willis, *Adv Mater,* **15**, 1161-1165 (2003).

[22] N. Grossiord, J. Loos, and C.E. Koning, *J. Mater. Chem.,* **15**, 2349-2352 (2005).

[23] D. Cai and M. Song, *Carbon,* **46**, 2107-2112 (2008).

[24] H.E. Miltner, N. Grossiord, K. Lu, J. Loos, C.E. Koning, and B. Van Mele, *Macromolecules,* **41**, 5753-5762 (2008).

[25] J.C. Grunlan, Y. Kim, S. Ziaee, X. Wei, B. Abdel-Magid, and K. Tao, *Macromol. Mater. Eng.,* **291**, 1035-1043 (2006).

[26] D.K. Woo, B.C. Kim, and S.J. Lee, *Korea-Aust. Rheol. J.,* **21**, 185-191 (2009).

[27] T.M. Wu and E.C. Chen, *Composites Sci. Technol.,* **68**, 2254-2259 (2008).

[28] J. Yu, K. Lu, E. Sourty, N. Grossiord, C.E. Koning, and J. Loos, *Carbon,* **45**, 2897-2903 (2007).

[29] P. Pötschke, A.R. Bhattacharyya, and A. Janke, *Polymer,* **44**, 8061-8069 (2003).

[30] J. Sandler, J. Kirk, I. Kinloch, M. Shaffer, and A. Windle, *Polymer,* **44**, 5893-5899 (2003).

[31] J. Sandler, M. Shaffer, T. Prasse, W. Bauhofer, K. Schulte, and A. Windle, *Polymer,* **40**, 5967-5971 (1999).

[32] R. Andrews, D. Jacques, D. Qian, and T. Rantell, *Acc. Chem. Res.,* **35**, 1008-1017 (2002).

[33] P. Kannan, R.J. Young, and S.J. Eichhorn, *Small,* **4**, 930-933 (2008).

[34] P. Apel, *Radiat. Measur.,* **34**, 559-566 (2001).

[35] P.Y. Apel, *Radiat. Measur.,* **25**, 667-674 (1995).

[36] C.R. Martin, *Chem. Mater.,* **8**, 1739-1746 (1996).

[37] I. Enculescu, *Digest J. Nanomater. Biostruct,* **1**, 15–20 (2006).

[38] P. Déjardin, E.N. Vasina, V. Vladimir, D. Vladimir, and V.I. Volkov, *Langmuir,* **21**, 4680-4685 (2005).

[39] E. Khataibe, T. Khokhlova, L. Trusov, and B. Mchedlishvili, *Colloid Journal,* **67**, 113-116 (2005).

[40] V. Berezkin, A. Nechaev, and N. Mitrofanova, *Colloid Journal,* **65**, 279-283 (2003).

[41] M. Chun, H. Il Cho, and I.K. Song, *Desalination,* **148**, 363-368 (2002).

[42] Z. Wang, C.J. Medforth, and J.A. Shelnutt, *J. Am. Chem. Soc.,* **126**, 15954-15955 (2004).

[43] A.D. Schwab, D.E. Smith, C.S. Rich, E.R. Young, W.F. Smith, and J.C. de Paula,*J. Phys. Chem. B,* **107**, 11339-11345 (2003).

[44] Z. Wang and J.A. Shelnutt,*J. Porphyr. Phthalocya.,* **8**, 578-578 (2004).

[45] S. Vlaming, R. Augulis, M. Stuart, J. Knoester, and P. Van Loosdrecht,*J. Phys. Chem. B,* **113**, 2273-2283 (2009).

[46] M.F. Kemmere, M.J.J. Mayer, J. Meuldijk, and A.A.H. Drinkenburg, *J Appl Polym Sci,* **71**, 2419-2422 (1999).

[47] A. Kathiravan and R. Renganathan, *Z. Phys. Chem.,* **222**, 987-995 (2008).

[48] P.A. de Witte, M. Castriciano, J.J. Cornelissen, L. Monsù Scolaro, R.J. Nolte, and A.E. Rowan, *Chem. Eur. J.,* **9**, 1775-1781 (2003).

[49] U. Sajeev, K.A. Anand, D. Menon, and S. Nair, *Bull. Mater. Sci.,* **31**, 343-351 (2008).

[50] J. Deitzel, J. Kleinmeyer, D.e.a. Harris, and N. Beck Tan, *Polymer,* **42**, 261-272 (2001).

PORPHYRIN NANORODS POTENTIAL APPLICATION

The next section is based on the non-linear optical investigations of porphyrin aggregates. This work has been published in the paper

Physical origin of third order non-linear optical response of porphyrin nanorods (N. Mongwaketsi, S. Khamlich, M. Pranaitis, B. Sahraoui, F. Khammarc, G. Garab, R. Sparrow, M. Maaza. Journal of Materials Chemistry and Physics. 134 (2010) 646-650).

5.1. Potential porphyrin nanorods application

5.1.1. Introduction

Porphyrins have great thermal stability and an extended π-conjugated macro cyclic ring which give them large nonlinear optical (NLO) effects. The NLO properties of these materials are of special interest, for energy transfer with molecular control [1]. The stability of mono- and dication porphyrin π-radicals makes these systems especially interesting for photoionization and photoconductive processes which are closely related to the so-called special-pair reaction center of photosynthesis and the photo-generation of electron transfer [2]. Novel NLO materials may not be obtained from simple monomeric porphyrins, but are produced when strong electronic interactions between porphyrins are induced by self-assembly to bring porphyrins close together or connecting their π-conjugation systems [3]. A nonlinear material exhibit strain, electric polarization, or magnetization response when it experiences stress, electric field, or magnetic field experienced. The third-order optical response of porphyrin nanorods was studied by second harmonic and third harmonic generation (SHG and THG respectively) techniques. The SHG is a nonlinear optical process whereby the photons interacting with a nonlinear material are added to form new photons with twice the energy. In THG process a light with tripled frequency is produced. For the measurements the studied nonlinear molecules must lack a centre of symmetry

to exhibit second order optical properties. These materials must also exhibit low optical losses and they must be photo- chemically stable as well as processable to be incorporated into devices [4]. The studied porphyrin nanorods showed interesting nonlinear optical behaviour as a result of mechanisms and processes at the molecular level. These porphyrin-based nanostructures may be used in molecular engineering where nonlinear response can exploited.

5.1.2. Materials and Methods

The second and third order NLO properties of porphyrin nanorods as thin films were investigated and the measurements were performed at room temperature by the maker fringes technique [5] for both *p* and *s* polarizations. Maker fringes are oscillations in the optical harmonic generated by a beam incident on a plane-parallel sample when the incidence angle is varied [6]. In this technique a laser beam is focused onto a non-linear sample of a certain length and the harmonic light is generated while the sample thickness is varied by rotating the sample [6]. A fused silica plate with nonlinear susceptibility of 2.0 x $10^{-22} m^2 / V^2$ was used as a reference material [7]. The samples were measured in glass cells with 1 and 2 mm path lengths using various incident laser beam energies for each sample.

5.1.3. Characterization technique

SHG and THG measurements were performed using a Q-switched Nd:YAG laser operating at the fundamental wavelength of 1064 nm with a 16 ps pulse duration and 10 Hz repetition rate. For THG an FL355 filter was used and an FL532 filter was used for the SHG experiments. There is a first beam splitter which is used to take off a weak part of the beam for synchronization of detection. The second one allows correcting of fundamental beam fluctuations. The half wave plate ($\lambda/2$) and the polarizer are also used in order to control the intensity of the incident beam.

5.1.4. Results and discussion

5.1.4.1. Porphyrin nanorods response to SGH and THG

The non-linear optical properties of porphyrin nanorods were investigated by SHG and THG experimental techniques and Figure 34 displays the respective spectra corresponding to the measured porphyrin nanorods samples. We observed that porphyrin nanorods exhibited both the second and third order nonlinear optical susceptibilities $\chi^{(2)}$ and $\chi^{(3)}$ respectively. The origin of this response is likely due to the interaction between neighbouring excited molecules, such as an exciton-exciton interaction [8].

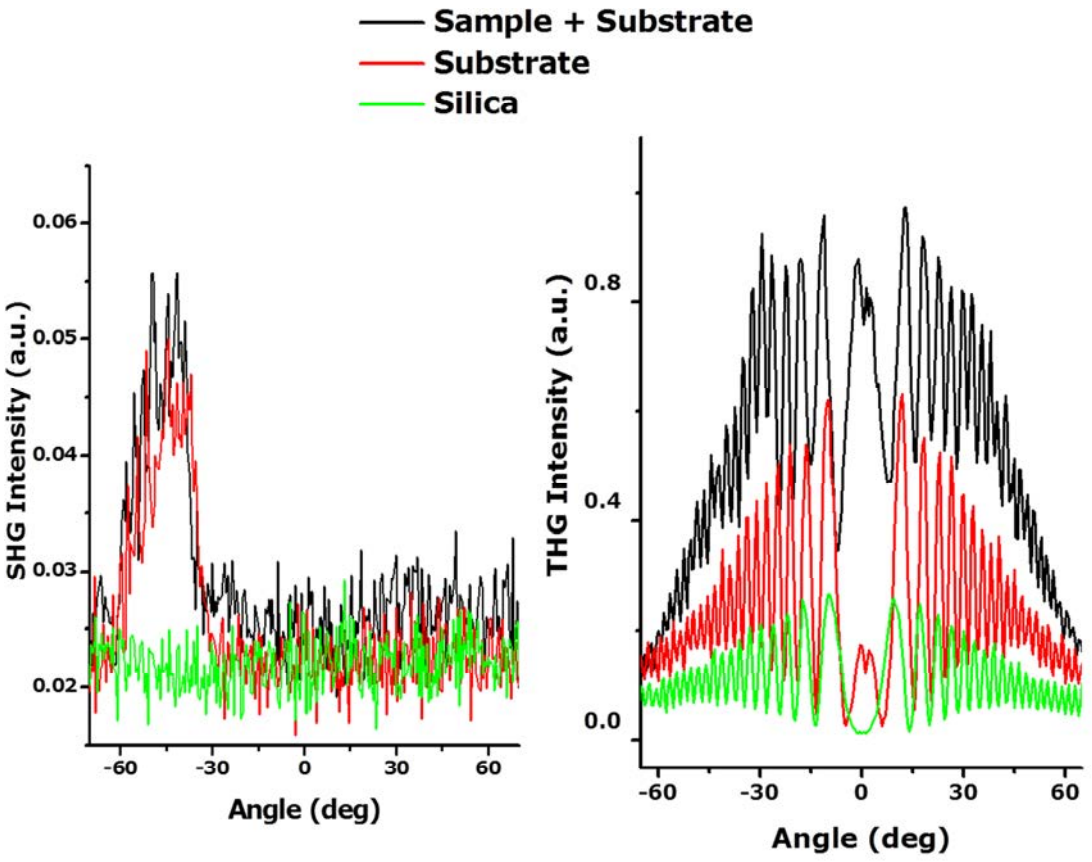

Figure 34. (a) SHG and (b) THF maker fringes signals as function of angle of incidence on the nanorods.

Further analyses were conducted on the THG results due to the improved porphyrin nanorods response to the procedure. Enhanced $\chi^{(3)}$ may be attributed to the strong coupling between porphyrin molecules during aggregation.The THG process provides information related only to the electronic contribution of the nonlinearity. The obtained THG data was analysed using a model of Kubodera and Kobayashi [9]. This model compares directly the maximal amplitudes of third harmonic light intensity of the studied sample to those of a reference material. For a weak absorption, the relation used to determine the χ^3 order of magnitude is given by the formula:

$$\frac{X^{<3>}}{X^{<3>}} = \frac{2}{\pi}\frac{L_{c,S}}{l}\sqrt{\frac{I^{3\omega}}{I_S{}^{3\omega}}} \qquad [2]$$

where:

$$L_c = \frac{\lambda_\omega}{6(n_{3\omega} - n_\omega)} \qquad [3]$$

Here $L_{c,S}$ – coherence length, l is thickness of sample (~500 nm), $I_S^{3\omega}$ and $I^{3\omega}$ are THG intensities of the silica and the studied material, respectively ($I^{3\omega}$= $I^{3\omega}_{[sample+substrate]}$ - $I^{3\omega}_{[substrate]}$), $n_{3\omega}$ = 1.476, n_ω= 1.449. This model compares directly the maximal amplitudes of third harmonic light intensity for studied material to those of a silica plate used as reference. $\chi^{(3)}_{silica}$ = 2.0×10^{-22} m^2/V^2 at λ_ω = 1064 nm. The $\chi^{(3)}$ results obtained are summarized in Table 5.

Table 5. The values of $\chi^{(3)}$ of the third harmonic generation measurements.

Sample	$\chi^{(3)}$, (10^{-21} m^2/V^2)
Fused Silica	0.2
H_2SO_4	1.37 ± 0.13
$H_2C_2O_4$	1.87 ± 0.18
H_3PO_4	1.12 ± 0.10
HNO_3	1.94 ± 0.10
HCl	2.01 ± 0.27

The redistribution among energy levels result in large non-linear response. However the response may be slow due to the redistribution time. The difference in the $\chi^{(3)}$ values could be either due to the redistribution time, different excited states in the solvent or to ground state absorption induced thermal effect. Porphyrins exhibit a strong excited state absorption from singlet and triplet lower excited states and this also contribute to the large $\chi^{(3)}$[10]. The steric hindrance and conformational disorder may also affect the π electron delocalization in porphyrin aggregates and can influence the nonlinear optical behaviour of the sample. The type of solvent used had an effect on the $\chi^{(3)}$ but with a very small difference between calculated values.

5.2. Conclusion

Non-linear optical properties of nanorods produced from the self-assembly of $H_4TPPS_4^{2-}$ and $SnTPyP^{2+}$ were measured for the first time using SHG and THG measurement systems. The experiments were performed in solutions, however, for practical applications, it is necessary to obtain processable materials, like thin solid films, in which the NLO properties of the active chromophores are preserved. The results obtained from studying the porphyrin aggregates in solutions have shown that there is an enhancement in the optical nonlinearity through population

of the excited state of the porphyrins leading to high third order nonlinear susceptibility. The NLO results from the study of $H_4TPPS_4^{2-}$ and $SnTPyP^{2+}$ aggregates indicated that they are promising potential components as light harvesters since materials with large third-order optical nonlinearities are considered to be promising candidates for photonic applications.

5.3. References

[1] M.O. Senge, M. Fazekas, E.G. Notaras, W.J. Blau, M. Zawadzka, O.B. Locos, and E.M. Ni Mhuircheartaigh, *Adv Mater,* **19**, 2737-2774 (2007).

[2] K.S. Suslick, N.A. Rakow, M.E. Kosal, and J.H. Chou,*J. Porphyr. Phthalocya.,* **4**, 407-413 (2000).

[3] K. Ogawa, C. Hara, and Y. Kobuke,*J. Porphyr. Phthalocya.,* **11**, 359-367 (2007).

[4] G. de la Torre, T. Torres, and F. Agulló-López, *Adv Mater,* **9**, 265-269 (1997).

[5] P. Maker, R. Terhune, M. Nisenoff, and C. Savage, *Phys. Rev. Lett.,* **8**, 21-22 (1962).

[6] I. Biaggio and M.S. Fleischman, *Opt. Lett.,* **38**, 4461-4464 (2013).

[7] F. Kajzar, Y. Okada-Shudo, C. Meritt, and Z. Kafafi, *Synth. Met.,* **117**, 189-193 (2001).

[8] M.K. Casstevens, M. Samoc, J. Pfleger, and P.N. Prasad, *J. Chem. Phys.,* **92**, 2019 (1990).

[9] K. Kubodera and H. Kobayashi, *Mol. Cryst. Liq. Cryst.,* **182**, 103-113 (1990).

[10] S.V. Rao, N. Srinivas, D.N. Rao, L. Giribabu, B.G. Maiya, R. Philip, and G.R. Kumar, *Opt. Commun.,* **182**, 255-264 (2000).

CONCLUSION

6.1.Overall conclusion and Recommendations

In summary, we successfully synthesized porphyrin-based nanorods and studied their optical properties as well as factors that influence the aggregation process. We found that these nanostructures displayed enhanced and similar characteristics of natural systems rendering them potential candidates as artificial light harvesting components.

We successfully incorporated the nanorods into polymer matrices and still preserved their morphology and optical properties. The latex blending produced composites with porphyrin nanostructures distributed on the surface and this approach allows one to control the properties of nanorods, the ability of which is expected to be useful for the fabrication of optical devices.

The surface coverage of the modified membranes using a layer-by-layer technique was maximized after only a few immersions, and the resulting modified membrane showed excellent absorbance signature which may be exploited in porphyrin based sensor or photonic applications. The electronic coupling present in these aggregates makes them potentially useful for application as antennae in synthetic light harvesting complexes.

Further work could be undertaken to investigate how altering the porphyrin monomers will affect the self-assembly performance and the properties of the resulting nanostructures. The orientation of porphyrin nanorods can be studied in future since the arrangement of the porphyrin dye molecules plays a key factor in realizing efficient light-harvesting arrays.

In our study the bonding properties and distribution characteristics of nanorods within porphyrin nanorods-polystyrene composites were investigated. The interfacial bonding needs to be investigated to determine the mechanical properties and tensile fracture mechanisms of porphyrin nanorods-polystyrene composites. Studies on fluorescence properties of fibres and maintenance of the performance of porphyrin nanorods in the systems is another area to be explored.

Alternative designs of light-harvesting systems where porphyrin pigments are organized in a three dimensional architecture such that light is absorbed strongly and the resulting excited state energy flows efficiently to a designated site could also be undertaken. Another possibility is to study the controllability of energy transfer *i.e*. produce a nanorods array where energy can be transferred from one site to another at a predetermined or designed time. In order to investigate the energy transfer processes of the designed systems Femtosecond pump probe transient absorption spectroscopy is recommended.